# Detecting OFDM Signals in Alpha-Stable Noise

Ahmed Mahmood, *Student Member, IEEE,* Mandar Chitre, *Senior Member, IEEE,*
and Marc Andre Armand, *Senior Member, IEEE*

***Abstract*—This paper analyzes various receiver schemes for orthogonal frequency division multiplexing (OFDM) transmission in impulsive noise. We consider Rayleigh block-fading and model the noise process by additive white symmetric $\alpha$-stable noise (AWS$\alpha$SN). We start-off by discussing maximum-likelihood (ML) detection performance of baseband OFDM. Though optimal, the computational cost increases exponentially with the number of carriers. Alternatively, one may evaluate soft-estimates of the transmitted symbol block and employ carrier-wise detection to lower computational complexity. We analyze such schemes under the frameworks of M-estimation and compressed sensing theory. Moving on, we highlight important rules that ensure the passband AWS$\alpha$SN process is converted to a baseband form suitable for the discussed schemes. Finally, it is shown that linear passband-to-baseband conversion actually reduces the signal-to-noise ratio (SNR) at the receiver and that all these rules may be avoided by applying an estimation scheme directly on the passband samples.**

***Index Terms*—OFDM, impulsive noise, AWS$\alpha$SN, ML, M-estimation, compressed sensing.**

## I. Introduction

IMPULSIVE noise is encountered in several practical scenarios, such as snapping shrimp noise in underwater channels [1], [2], communication over powerlines [3], [4], digital subscriber lines [5], [6] etc. Though not as widespread as thermal noise, its effect on a digital receiver is severe if not countered [2], [7]. A noise realization is impulsive if sudden 'spikes' in magnitude (or outliers) are observed. Due to this phenomenon, Gaussian distributions fail to model the noise process efficiently [8]. In the literature, various models have been employed to simulate impulsive noise [2], [9], [10]. We consider the additive white symmetric $\alpha$-stable noise (AWS$\alpha$SN) model for all of our analysis.

The AWS$\alpha$SN model is based on heavy-tailed symmetric $\alpha$-stable (S$\alpha$S) distributions. The motivation of using AWS$\alpha$SN stems from the generalized central limit theorem (GCLT), which states that the sum of independent and identically distributed (IID) random variables tends to a *stable* distribution as the number of elements in the sum tends to infinity [8], [11], [12]. A stable distribution is S$\alpha$S if its probability density function (PDF) is *symmetric* about zero. As the central limit theorem (CLT) is merely the GCLT with an added power constraint, the zero-mean Gaussian distribution is implicitly S$\alpha$S [11], [12]. With the exception of the Gaussian case, all S$\alpha$S members are heavy-tailed. This characteristic allows them to model outliers very well [8].

Orthogonal frequency division multiplexing (OFDM) is increasingly being adopted as a physical-layer modulation scheme in new and emerging wireless standards [13]. It has a number of good properties such as high spectral efficiency, cost-efficient implementation using the fast Fourier transform (FFT), conversion of an $N$-tap frequency-selective channel into $N$ parallel flat-fading channels [13] etc. Adding to this list, it was recently shown that the error performance in AWS$\alpha$SN and Rayleigh block-fading actually *improves* under maximum-likelihood (ML) detection by *increasing* the number of carriers in an OFDM system [14]. This is attributed to the fact that the information within an impulse is distributed over a bandwidth larger than that of any sub-carrier. In turn, joint-detection harnesses this information from all available carriers. The performance gain over a single-carrier scheme is significant. However, the complexity of performing joint-detection at the receiver increases exponentially with the number of carriers, thus rendering this approach unfeasible.

In the literature, besides ML detection, several solutions to the impulsive noise problem have been suggested [15]–[17]. The typical approach is to retrieve information about the location (and magnitude) of impulses from the received observations and use them to evaluate robust estimates of the transmitted data. Structural similarities between an OFDM codeword and Reed-Solomon codes were exploited in [17], [18]. The scheme used pilots and nulls within the OFDM block to estimate the locations and magnitudes of the impulses in the noise realization. In [19], the authors took advantage of the inherent sparsity of impulsive noise and employed compressed sensing (CS) to estimate the noise realization. Both of the aforementioned schemes were analyzed for the baseband Gaussian-Bernoulli-Gaussian (GBG) channel and adopt a noise-cancellation approach after which conventional (Euclidean) detection is employed to retrieve the transmitted data. However, the latter scheme finds a solution relatively quicker as it employs powerful yet computationally efficient convex programs to generate the estimates [20].

There are three main contributions in this paper. Firstly, we provide insight to the relationship between the ML detection results for OFDM in [14] and the CS approach in [19]. A thorough analysis of the results and trends is conducted in the presence of Rayleigh block-fading and impulsive noise. Secondly, one of the main assumptions in the related literature is that the baseband noise is impulsive (and therefore sparse). Though the passband AWS$\alpha$SN process for $\alpha \neq 2$ is sparse, this *does not* guarantee sparsity in the baseband. Building on [7], we highlight the design constraints within a linear

A. Mahmood is with the ARL, Tropical Marine Science Institute, National University of Singapore, Singapore 119227, Singapore (e-mail: tmsahme@nus.edu.sg)

M. Chitre is with the Department of Electrical and Computer Engineering and the ARL, Tropical Marine Science Institute, National University of Singapore, Singapore 119227, Singapore (e-mail: mandar@nus.edu.sg)

M. A. Armand is with the Department of Electrical and Computer Engineering, National University of Singapore, Singapore 117576, Singapore (e-mail: eleama@nus.edu.sg )

Manuscript received April 9, 2014; revised July 7, 2014.

passband-to-baseband conversion block that are sufficient to induce sparsity in the baseband noise vector. Lastly, it is shown that linear passband-to-baseband conversion is suboptimal and reduces the signal-to-noise ratio (SNR) at the receiver. In certain scenarios, such as underwater acoustic communications, the carrier frequency is low. Therefore the transmitted symbol block can be estimated directly from the passband samples. We derive such a scheme and show that it completely avoids the SNR reduction caused by the linear passband-to-baseband conversion block.

This paper is organized as follows: In Section II we summarize related concepts and research in the literature. Section III analyzes the pros and cons of ML joint-detection for baseband OFDM in impulsive noise with Rayleigh block-fading. In Section IV we discuss the $L_p$-norm and CS approaches to decoding baseband OFDM signals under the framework of M-estimation theory. Given passband AWS$\alpha$SN and linear passband-to-baseband conversion, the baseband noise vector can take over a large number of statistical configurations when $\alpha \neq 2$ [7]. In Section V, we highlight design rules within the linear framework that guarantee a sparse baseband noise vector. Taking note that baseband conversion is not optimal in non-Gaussian AWS$\alpha$SN, we show in Section VI that the passband transmit-receive equation can be expressed in a somewhat similar form to its baseband counterpart and may be processed via the mechanisms discussed in Section IV. Finally, we summarize our contributions in Section VII.

## II. Concepts

### A. S$\alpha$S Distributions

A *symmetric* random *variable* $X$ is S$\alpha$S if and only if

$$\sum_{i=1}^{K} a_i X^{(i)} \stackrel{d}{=} cX \tag{1}$$

where $a_i, c \in \mathbb{R}$, $K \in \mathbb{Z}^+$ and $X^{(i)}\ \forall\ i \in \{1, 2, \ldots, K\}$ are independent and identically distributed (IID) copies of $X$ [8], [11], [12]. The symbol $\stackrel{d}{=}$ implies *equality in distribution* [8]. On further inspection, (1) implies that any *linear* combination of independent S$\alpha$S random variables results in an S$\alpha$S distribution. This *stability property* is uniquely attributed to stable distributions. An S$\alpha$S PDF is completely characterized by its characteristic exponent $\alpha \in (0, 2]$ and scale parameter $\delta \in (0, +\infty)$ [8]. Therefore, the corresponding distribution may be succinctly defined by the notation $X \sim \mathcal{S}(\alpha, \delta)$ [7]. In (1), the relationship between the coefficients is given by

$$c = \left( \sum_{i=1}^{K} |a_i|^{\alpha} \right)^{1/\alpha}, \tag{2}$$

i.e., $c$ is the $L_\alpha$-norm of the $K$-tuple $[a_1, a_2, \ldots, a_K]$.

Well-known members of the S$\alpha$S family include the zero-mean Gaussian distribution $\mathcal{S}(2, \delta)$ (equivalent to $\mathcal{N}(0, 2\delta^2)$) and the zero-median Cauchy distribution $\mathcal{S}(1, \delta)$ [8], [11]. Though the Gaussian and non-Gaussian cases share some similarities (like the stability property in (1)), they are strikingly different in many aspects. For example, second-order moments of non-Gaussian S$\alpha$S distributions are infinite [8], [11], [12]. Therefore, analysis methods involving variances or correlations that are typically employed in Gaussian scenarios do not extend to the general S$\alpha$S case. Likewise, with the exception of the Gaussian case, S$\alpha$S distributions have algebraic (heavy) tails. As $\alpha \to 0$, the tails get increasingly heavier [8], [11], [12]. Further still, PDFs of the S$\alpha$S family generally cannot be expressed in closed-form. The Gaussian and Cauchy members, however, are exceptions to this rule. When working with such PDFs, one may need to revert to numerical techniques or analytic approximations [8], [21], [22].

We can extend the definition in (1) to incorporate S$\alpha$S *vectors*, i.e., if $\mathbf{x}^{(i)}$ are IID copies of a symmetric random vector $\mathbf{x}$, then

$$\sum_{i=1}^{K} a_i \mathbf{x}^{(i)} \stackrel{d}{=} c\mathbf{x} \tag{3}$$

where $a_i, c \in \mathbb{R}$, $K \in \mathbb{Z}^+$. The equality in (2) also extends to the coefficients in (3).

For the special case of $\mathbf{x}$ with IID $\mathcal{S}(\alpha, \delta)$ components, $\mathbf{x}$ is S$\alpha$S. This is observed by noting that each element of $\mathbf{x}$ satisfies (1) with the *same set* of coefficients, and therefore, (3) will hold. Any *complex* random variable can be written as a 2-dimensional *real* random vector [23]. Similarly, an $N$-dimensional complex random vector can be expressed as a $2N$-dimensional real vector. If $\mathbf{x}_c \in \mathbb{C}^N$, then we say it is S$\alpha$S if (3) holds for $\mathbf{x} = [\Re\{\mathbf{x}_c\}^\mathsf{T}\ \Im\{\mathbf{x}_c\}^\mathsf{T}]^\mathsf{T} \in \mathbb{R}^{2N}$.

### B. The AWS$\alpha$SN Model

By definition, the samples of an AWS$\alpha$SN process are real IID S$\alpha$S random variables [2], [7]. This implicitly implies that the process is stationary. When $\alpha = 2$, AWS$\alpha$SN is equivalent to the well-known AWGN process. Though AWGN has a flat (or white) power spectral density (PSD), the same definition does not extend to non-Gaussian AWS$\alpha$SN as second-order moments of its samples are infinite [8]. This implies that the corresponding PSD is infinite as well. The term 'white' is retained to highlight the IID nature of the samples instead [7].

Another characteristic of non-Gaussian AWS$\alpha$SN is that its realizations are 'impulsive', i.e., the magnitude of a *few* samples are significantly larger than the rest. This is a direct consequence of the heavy-tails associated with the S$\alpha$S family and therefore the realizations are *sparse* [8]. If the samples are each distributed as $\mathcal{S}(\alpha, \delta)$, the degree of impulsiveness is determined by $\alpha$. Lowering $\alpha$ makes the process increasingly impulsive, i.e., the relative magnitude of the significant samples increase with respect to the rest. On the other hand, $\delta$ merely scales all the samples in the realization and does not increase the impulsiveness of the noise process.

### C. The Baseband OFDM System Model

In digital communications, analysis is typically performed in the baseband [24], [25]. Let $\mathbf{z} = [z_1, z_2, \ldots, z_N]^\mathsf{T}$ be the complex noise vector, i.e., $\mathbf{z} \in \mathbb{C}^N$. Also define $\mathbf{x} = [x_1, x_2, \ldots, x_N]^\mathsf{T}$ as the $N \times 1$ OFDM symbol vector and $\mathbf{A} = [\mathbf{a}_1, \mathbf{a}_2, \ldots, \mathbf{a}_N]$ the $N$-point *unitary* discrete Fourier transform (DFT) matrix with columns $\mathbf{a}_k$. Each $x_k\ \forall\ k \in$

$\{1, 2, \ldots, N\}$ is selected from an $M$-ary constellation. The baseband transmit-receive OFDM equation is then

$$\mathbf{y} = \mathbf{H}_c \mathbf{A}^{\mathsf{H}} \mathbf{x} + \mathbf{z} \tag{4}$$

where $\mathbf{y} = [y_1, y_2, \ldots, y_N]^{\mathsf{T}}$ is the received vector and $\mathbf{H}_c$ is the $N \times N$ complex circulant channel matrix. We consider zero-Doppler and Rayleigh block fading, therefore, $\mathbf{H}_c$ is time-invariant. From the properties of $\mathbf{A}$ and $\mathbf{H}_c$, the latter can be diagonalized by $\mathbf{H} = \mathbf{A}\mathbf{H}_c\mathbf{A}^{\mathsf{H}}$, where $\mathbf{H} = \mathtt{diag}[h_1, h_2, \ldots, h_N]$ [13], [26]. We can thus rewrite (4) as

$$\mathbf{y} = \mathbf{A}^{\mathsf{H}} \mathbf{H} \mathbf{x} + \mathbf{z} \tag{5}$$

where $h_k \sim \mathcal{CN}(0, \sigma_h^2) \ \forall \ k \in \{1, 2, \ldots, N\}$ are circularly symmetric complex Gaussian random variables with mean 0 and variance $\sigma_h^2$. Also, all $h_k$ are IID. Typically, an OFDM symbol block consists of data, pilots and nulls. The locations of these within $\mathbf{x}$ are known. For our analysis in this paper, we use $0 < K \leq N$ data-carriers and $N - K$ nulls. As the pilots are known, they can easily be accommodated within our problem formulation. We discuss this briefly in Section IV. Also, the receiver is assumed to have *complete knowledge* of the channel.

Eq. (5) can be expressed in terms of only the actual transmitted data. Defining $\mathcal{L}_{\mathbf{x}} = \{\ell_1, \ell_2, \ldots, \ell_K\}$ as the set whose elements are the locations (indices) of the data symbols in $\mathbf{x}$ and $\mathbf{x}_{(1)} = [x_{\ell_1}, x_{\ell_2}, \ldots, x_{\ell_K}]^{\mathsf{T}}$ as the $K$-tuple data vector, we have from (5)

$$\mathbf{y} = \bar{\mathbf{A}}^{\mathsf{H}} \bar{\mathbf{H}} \mathbf{x}_{(1)} + \mathbf{z} \tag{6}$$

where $\bar{\mathbf{A}}^{\mathsf{H}} = [\mathbf{a}_{\ell_1}^*, \mathbf{a}_{\ell_2}^*, \ldots, \mathbf{a}_{\ell_K}^*]$ is of size $N \times K$ and $\bar{\mathbf{H}} = \mathtt{diag}[h_{\ell_1}, h_{\ell_2}, \ldots, h_{\ell_K}]$. The notation $\mathbf{a}_{\ell_1}^*$ denotes the complex conjugate of all elements in the vector $\mathbf{a}_{\ell_1}$. Similarly, we can combine the columns of $\mathbf{A}^{\mathsf{H}}$ whose indices are not in $\mathcal{L}_{\mathbf{x}}$ to form the $N \times (N - K)$ matrix $\bar{\bar{\mathbf{A}}}^{\mathsf{H}}$. These columns correspond to the position of the nulls in $\mathbf{x}$. As the columns of $\mathbf{A}$ are orthonormal, we get

$$\begin{aligned} &\bar{\mathbf{A}}\bar{\mathbf{A}}^{\mathsf{H}} = \mathbf{I}_K, \\ &\bar{\bar{\mathbf{A}}}\bar{\bar{\mathbf{A}}}^{\mathsf{H}} = \mathbf{I}_{N-K} \text{ and} \\ &\bar{\mathbf{A}}\bar{\bar{\mathbf{A}}}^{\mathsf{H}} = \mathbf{0}_{K \times (N-K)}. \end{aligned} \tag{7}$$

where $\mathbf{I}_K$ and $\mathbf{0}_{K \times (N-K)}$ represent the $K \times K$ identity matrix and the $K \times (N - K)$ all-zero matrix, respectively. The statistical characteristics of $\mathbf{z}$ will be briefly discussed next.

### *D. Characterization of the Complex Noise Vector in AWS$\alpha$SN*

A typical passband-to-baseband conversion block is a linear system which retains in-band information [7], [25]. This is optimal (in the ML sense) for AWGN and may be implemented in either continuous-time or on a non-lossy sampled version of the passband signal. Regardless of the implementation, the statistics of $\mathbf{z}$ *do not* change for passband AWGN. If the double-sided noise PSD is $N_0/2$, then $z_n \ \forall \ n \in \{1, 2, \ldots, N\}$ are IID random variables and are each distributed by $\mathcal{CN}(0, N_0)$. This implies that $\mathbf{z}$ is *isotropic* [25]. Due to these properties, without losing any information of the noise component contaminating $\mathbf{x}_{(1)}$, one may multiply (6) with $\bar{\mathbf{A}}$ to get

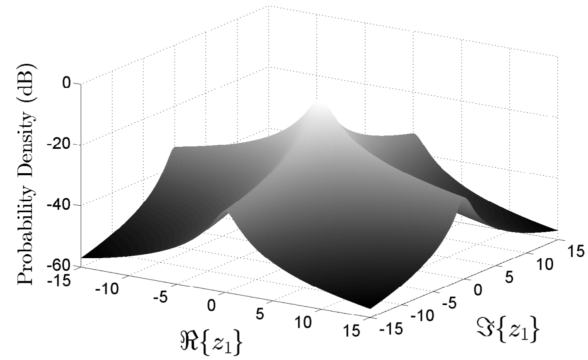


Fig. 1. The bivariate pdf of a standard Cauchy $\mathbf{z} \stackrel{d}{=} \mathbf{z}_{\text{IID}}$ for $N = 1$.

$$\acute{\mathbf{y}} = \bar{\mathbf{H}} \mathbf{x}_{(1)} + \acute{\mathbf{z}}. \tag{8}$$

Here $\acute{\mathbf{y}} = \bar{\mathbf{A}}\mathbf{y}$ and $\acute{\mathbf{z}} = \bar{\mathbf{A}}\mathbf{z}$. The elements of $\acute{\mathbf{z}}$ are also $\mathcal{CN}(0, N_0)$ and independent due to the orthonormal columns of $\mathbf{A}$ [13].

If non-Gaussian AWS$\alpha$SN is passed through a linear passband-to-baseband conversion block, the statistics of $\mathbf{z}$ vary significantly with the passband sampling frequency [7], [27]. The resulting distribution, however, will always be S$\alpha$S. Of all possible distributions, the case of $\mathbf{z}$ with IID real and imaginary components offers the best error performance [7], [27]. In such a case, $\Re\{z_m\} \stackrel{d}{=} \Im\{z_n\} \stackrel{d}{=} Z \sim \mathcal{S}(\alpha, \delta_z) \ \forall \ m, n \in \{1, 2, \ldots, N\}$ and are mutually independent. Though this implies isotropy if $\mathbf{z}$ is Gaussian, this is not the case when $\alpha \neq 2$. In fact, the joint-PDF of $\mathbf{z}$ has discrete 'tails' directed along the positive and negative directions of each coordinate axis [7]. We term this configuration of $\mathbf{z}$ as $\mathbf{z}_{\text{IID}}$. An instance of this is plotted in Fig. 1 for the Cauchy case with $N = 1$. One can clearly see that their are four tails in the PDF directed along the positive and negative directions of both the $\Re\{z_1\}$ and $\Im\{z_1\}$ axis.

If a continuous-time implementation of the linear passband-to-baseband conversion block is adopted, then $z_n$ is a complex isotropic S$\alpha$S random variable [7], [27]. In such a case, $\Re\{z_n\}$ and $\Im\{z_n\}$ are *dependent* for any $n$ [8]. Further still, the components of $\mathbf{z}$ are *identical*. Therefore, $\Re\{z_m\} \stackrel{d}{=} \Im\{z_n\} \stackrel{d}{=} Z \sim \mathcal{S}(\alpha, \delta_z) \ \forall \ m, n \in \{1, 2, \ldots, N\}$ [8]. We denote $\mathbf{z}$ with IID components and per-carrier isotropy as $\mathbf{z}_{\text{ISO}}$. Note that this is *not* equivalent to defining $\mathbf{z}$ as an isotropic random vector, as the latter (unlike $\mathbf{z}_{\text{ISO}}$) *cannot* have independent components [8], [11]. The dependency within the components of $\mathbf{z}$ can actually be varied by changing the configuration of the low-pass filter in the passband-to-baseband conversion block [27]. This is discussed in detail in Section V-B.

In the literature, baseband analysis in impulsive noise has been conducted both for $\mathbf{z}_{\text{IID}}$ and $\mathbf{z}_{\text{ISO}}$ [17], [28], [29]. Though our primary focus is on the prior, we discuss results for both throughout the paper to see their similarities and differences.

## III. ML Detection of OFDM Signals in AWS$\alpha$SN

In this section, we briefly summarize the ML detection results offered for the $\mathbf{z} \overset{d}{=} \mathbf{z}_{\text{IID}}$ case in [14]. We show results for the $\mathbf{z} \overset{d}{=} \mathbf{z}_{\text{ISO}}$ case as well.

The ML detection rule of the OFDM symbol block in (6) is given by

$$\hat{\mathbf{x}}_{(1)} = \underset{\boldsymbol{\zeta}\in\mathbb{S}}{\texttt{arg max}}\; f_{\mathbf{z}}(\mathbf{y} - \bar{\mathbf{A}}^{\mathsf{H}}\bar{\mathbf{H}}\boldsymbol{\zeta}) \tag{9}$$

where $f_{\mathbf{z}}(\cdot)$ is the $2N$-dimensional joint-PDF of $\mathbf{z}$ and $\mathbb{S}$ is the set of all possible OFDM symbols such that $\mathbf{x}_{(1)} \in \mathbb{S}$. Given that $\mathbf{z} \overset{d}{=} \mathbf{z}_{\text{IID}}$ and denoting $\bar{\mathbf{A}} = [\bar{\mathbf{a}}_1, \bar{\mathbf{a}}_2, \ldots, \bar{\mathbf{a}}_N]$, we have

$$\hat{\mathbf{x}}_{(1)} = \underset{\boldsymbol{\zeta}\in\mathbb{S}}{\texttt{arg max}} \prod_{n=1}^{N} f_z(y_n - \bar{\mathbf{a}}_n^{\mathsf{H}}\bar{\mathbf{H}}\boldsymbol{\zeta}) \tag{10}$$

$$= \underset{\boldsymbol{\zeta}\in\mathbb{S}}{\texttt{arg min}} \sum_{n=1}^{N} -\log f_z(y_n - \bar{\mathbf{a}}_n^{\mathsf{H}}\bar{\mathbf{H}}\boldsymbol{\zeta}) \tag{11}$$

where $f_z(\cdot) = f_Z(\Re\{\cdot\})f_Z(\Im\{\cdot\})$ is the bivariate PDF of $z_n \;\forall\; n \in \{1, 2, \ldots, N\}$ and $\log(\cdot)$ is the *natural logarithm*. The expressions in (10) and (11) are equivalent as the cost function in (10) is strictly positive and $\log(\cdot)$ is a monotonically increasing function in this domain.

For the Gaussian case, (11) may be simplified further. From (8), we have

$$\hat{\mathbf{x}}_{(1)} = \underset{\boldsymbol{\zeta}\in\mathbb{S}}{\texttt{arg max}}\; f_{\mathbf{z}}(\acute{\mathbf{y}} - \bar{\mathbf{H}}\boldsymbol{\zeta})$$

$$= \underset{\boldsymbol{\zeta}\in\mathbb{S}}{\texttt{arg min}} \sum_{k=1}^{K} -\log f_z(\acute{y}_k - h_{\ell_k}\zeta_k)$$

$$= \underset{\boldsymbol{\zeta}\in\mathbb{S}}{\texttt{arg min}} \sum_{k=1}^{K} |\acute{y}_k - h_{\ell_k}\zeta_k|^2 \tag{12}$$

where $\acute{\mathbf{y}} = [\acute{y}_1, \acute{y}_2, \ldots, \acute{y}_K]^{\mathsf{T}}$, $\boldsymbol{\zeta} = [\zeta_1, \zeta_2, \ldots, \zeta_K]^{\mathsf{T}}$ and $\|\cdot\|$ is the Euclidean norm. In fact, (12) is the ML-detection rule for *any* unimodal isotropic $\acute{\mathbf{z}}$ as its PDF is a monotonically decreasing function of $\|\acute{\mathbf{z}}\|$. Though (12) is a combinatorial problem, the computational cost increases linearly with the number of carriers [13]. This is because the cost function is a sum of individual terms for each $k$ and therefore each term can be independently minimized. Thus, evaluating (12) is easy to perform even for moderately large $N$. Do note that the cost function in (11) is a sum of $N$ elements, while that in (12) is a sum of $K$. This is due to the fact that the information in the null carriers is irrelevant for the Gaussian case, but not in general.

In [14], performance analysis of ML-detection was conducted for S$\alpha$S $\mathbf{z} \overset{d}{=} \mathbf{z}_{\text{IID}}$. All carriers in the system were reserved for data, i.e., $K = N$. It was shown that the detection performance actually improves by increasing $N$. In fact, the error curves approach the ML-detection performance in isotropic Gaussian $\mathbf{z}$. To highlight these trends, we plot the bit error rate (BER) for various $N$ and $\alpha = 1$ in Fig. 2 along with the Gaussian error curve. The per-carrier constellation is BPSK and we employ the following SNR measure

$$\text{SNR}_{\text{dB}} = 10\log_{10}\frac{\mathcal{E}_x\sigma_h^2}{4\delta_z^2\log_2 M} \tag{13}$$

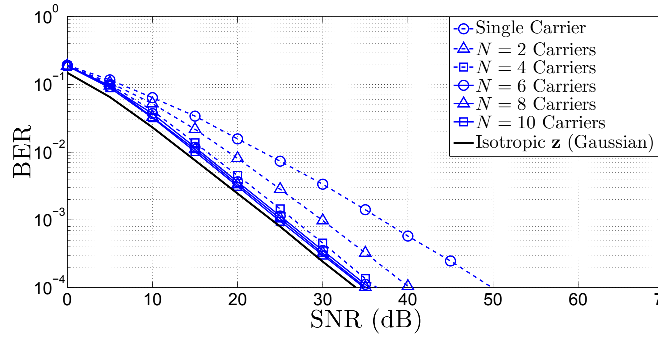


Fig. 2. ML BER performance averaged over $\bar{\mathbf{H}}$ for Cauchy $\mathbf{z} \overset{d}{=} \mathbf{z}_{\text{IID}}$. The curves are generated for various $N = K$ with per-carrier constellation BPSK.

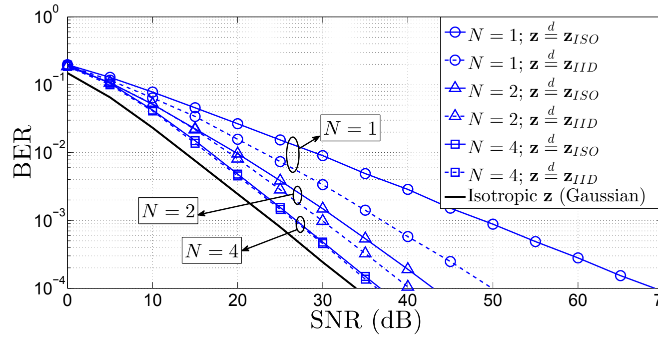


Fig. 3. ML BER performance averaged over $\bar{\mathbf{H}}$ for Cauchy $\mathbf{z} \overset{d}{=} \mathbf{z}_{\text{ISO}}$ (solid lines). The curves are generated for various $N = K$ with per-carrier constellation BPSK and compared with those in Fig. 2 (dashed lines).

where $\mathcal{E}_x = E[\|\mathbf{x}\|^2]/K$ is the average energy per-carrier. This measure is selected because it reduces to the well-known SNR per-bit $\mathcal{E}_x\sigma_h^2/(N_0\log_2 M)$ for the Gaussian case. Due to their common heavy-tailed property, the trends in Fig. 2 may be intuitively extended to any S$\alpha$S $\mathbf{z} \overset{d}{=} \mathbf{z}_{\text{IID}}$ for $\alpha \neq 2$.

In Fig. 3, we compare the BER for $\mathbf{z} \overset{d}{=} \mathbf{z}_{\text{ISO}}$ to their counterparts in Fig. 2. Remember that $f_z(\cdot)$ has algebraic tails when $z$ is non-Gaussian S$\alpha$S and therefore is an *algebraic function* of $\|\cdot\|$ due to the isotropy when $\mathbf{z} \overset{d}{=} \mathbf{z}_{\text{ISO}}$. Further still, $f_z(\cdot)$ is a monotonically decreasing function of $\|\cdot\|$. The rule in (11) then simplifies to

$$\hat{\mathbf{x}}_{(1)} = \underset{\boldsymbol{\zeta}\in\mathbb{S}}{\texttt{arg min}} \sum_{n=1}^{N} \log|y_n - \bar{\mathbf{a}}_n^{\mathsf{H}}\bar{\mathbf{H}}\boldsymbol{\zeta}|^2. \tag{14}$$

One can clearly see the performance difference between the two statistical configurations of $\mathbf{z}$ especially when $N = 1$ and $N = 2$. Further still, for $N = 4$ the error performance is almost identical, implying that $\mathbf{z}_{\text{IID}}$ and $\mathbf{z}_{\text{ISO}}$ offer almost equal information about the impulses under ML detection. In either case, however, there is a remarkable improvement in error performance in comparison to their single-carrier ($N = 1$) counterpart. This is clearly observed even for small $N > 1$. The increase in performance is attributed to the fact that the DFT operation spreads the transmitted information amongst the carriers. If a received sample is affected by an impulse, joint-detection takes advantage of the spread in information to output more robust estimates of the transmitted symbol block.

In a single-carrier system, signal constellations need to be designed specifically to take advantage of the noise anisotropy to enhance performance [27]. Baseband constellations are typically designed for the isotropic (Gaussian) case and cannot be blindly used for $\mathbf{z} \stackrel{d}{=} \mathbf{z}_{\text{IID}}$. However, in OFDM, the dependence on the constellation structure actually *reduces* with increasing $N$ [14]. This is mainly due to the channel matrix $\mathbf{H}$ which randomly introduces phase and magnitude to the transmitted symbols on each sub-carrier and the averaging effect of joint-detection.

A problem associated with the ML-detection rules in (11) and (14) is that the computational-cost increases exponentially with $K$. This is not an issue when $K$ is small. In (11), the issue is further augmented due to the non-availability of closed-form S$\alpha$S PDFs. Therefore, estimating $\mathbf{x}_{(1)}$ for large $K$ becomes computationally inefficient and eventually, intractable. Further still, one needs to estimate $\alpha$ and $\delta$ associated with $z_n$ before ML detection can be truly applied. In the next section, we outline an approach that is not only unhampered by these problems but (under some constraints) results in near-ML performance when $K$ is large.

## IV. Baseband OFDM Receiver Design

Our analysis will be primarily based on $\mathbf{z} \stackrel{d}{=} \mathbf{z}_{\text{IID}}$. We use the results to comment on the $\mathbf{z} \stackrel{d}{=} \mathbf{z}_{\text{ISO}}$ case as well.

### A. Problem Formulation

Instead of performing detection directly in (11), one can first try to evaluate *soft-estimates* of $\mathbf{x}_{(1)}$. The detection stage may then be employed subsequently. We can modify (11) to get the ML *estimate* of $\mathbf{x}_{(1)}$:

$$\hat{\mathbf{x}}_{(1)} = \underset{\boldsymbol{\mu}\in\mathbb{C}^K}{\arg\min} \sum_{n=1}^{N} -\log f_z(y_n - \bar{\mathbf{a}}_n^{\mathsf{H}}\bar{\mathbf{H}}\boldsymbol{\mu}). \tag{15}$$

Do note how $\boldsymbol{\mu}$ spans the entire $\mathbb{C}^K$ space, and therefore $\hat{\mathbf{x}}_{(1)} \in \mathbb{C}^K$. This is in contrast to (11) where $\hat{\mathbf{x}}_{(1)} \in \mathbb{S}$. By using a change of variables $\gamma_n = y_n - \bar{\mathbf{a}}_n^{\mathsf{H}}\bar{\mathbf{H}}\boldsymbol{\mu}$, we can convert the unconstrained problem in (15) into a constrained one with linear equalities:

$$\begin{aligned} \hat{\mathbf{x}}_{(1)}, \hat{\mathbf{z}} = \quad & \underset{\boldsymbol{\mu},\boldsymbol{\gamma}}{\arg\min} \quad \textstyle\sum_{n=1}^{N} -\log f_z(\gamma_n) \\ & \texttt{s.t.} \quad \mathbf{y} = \bar{\mathbf{A}}^{\mathsf{H}}\bar{\mathbf{H}}\boldsymbol{\mu} + \boldsymbol{\gamma}. \end{aligned} \tag{16}$$

Here $\gamma_n$ is the $n^{th}$ element of $\boldsymbol{\gamma} \in \mathbb{C}^N$. The vector $\boldsymbol{\gamma} = \hat{\mathbf{z}}$ is an estimate of $\mathbf{z}$, and along with $\boldsymbol{\mu} = \hat{\mathbf{x}}_{(1)}$, minimizes the cost function in (16). As any one-to-one mapping of the constraints (or cost-function) does not influence the minimization process [20], we may express (16) as

$$\begin{aligned} \hat{\mathbf{x}}_{(1)}, \hat{\mathbf{z}} = \quad & \underset{\boldsymbol{\mu},\boldsymbol{\gamma}}{\arg\min} \quad \textstyle\sum_{n=1}^{N} -\log f_z(\gamma_n) \\ & \texttt{s.t.} \quad \mathbf{A}\mathbf{y} = \mathbf{A}\bar{\mathbf{A}}^{\mathsf{H}}\bar{\mathbf{H}}\boldsymbol{\mu} + \mathbf{A}\boldsymbol{\gamma}. \end{aligned} \tag{17}$$

From the equalities in (7), we can further simplify (17) to

$$\begin{aligned} \hat{\mathbf{x}}_{(1)}, \hat{\mathbf{z}} = \quad & \underset{\boldsymbol{\mu},\boldsymbol{\gamma}}{\arg\min} \quad \textstyle\sum_{n=1}^{N} -\log f_z(\gamma_n) \\ & \texttt{s.t.} \quad \bar{\mathbf{A}}\mathbf{y} = \bar{\mathbf{H}}\boldsymbol{\mu} + \bar{\mathbf{A}}\boldsymbol{\gamma} \\ & \qquad\ \ \bar{\bar{\mathbf{A}}}\mathbf{y} = \bar{\bar{\mathbf{A}}}\boldsymbol{\gamma}. \end{aligned} \tag{18}$$

Do note that there are two sets of equalities in (18); the first consists of the data vector and the latter just the nulls. We can express $\hat{\mathbf{x}}_{(1)}$ explicitly in terms of $\mathbf{x}_{(1)}$ and the estimation error $\mathbf{e}$. From (6) and $\mathbf{y} = \bar{\mathbf{A}}^{\mathsf{H}}\bar{\mathbf{H}}\hat{\mathbf{x}}_{(1)} + \hat{\mathbf{z}}$, we have

$$\begin{aligned} \hat{\mathbf{x}}_{(1)} &= \bar{\mathbf{H}}^{-1}\bar{\mathbf{A}}\,(\mathbf{y} - \hat{\mathbf{z}}) \\ &= \mathbf{x}_{(1)} + \underbrace{\bar{\mathbf{H}}^{-1}\bar{\mathbf{A}}\,(\mathbf{z} - \hat{\mathbf{z}})}_{\text{estimation error}} \\ &= \mathbf{x}_{(1)} + \mathbf{e}. \end{aligned} \tag{19}$$

ML estimation theory in reference to stable distributions and their parameterizations have been covered well in [30]–[32]. Under certain regularity conditions, the limiting properties generally associated with ML estimates extend to stable parameters: they are efficient, consistent and asymptotically normal [33]. In the limit $N \to \infty$, $\mathbf{e}$ is a circularly symmetric complex Gaussian vector such that

$$\mathbf{e} \sim \mathcal{CN}(\mathbf{0}_{K\times 1}, \frac{2\delta_z^2}{\mathcal{I}^{(0)}}(\bar{\mathbf{H}}^{\mathsf{H}}\bar{\mathbf{H}})^{-1}), \tag{20}$$

where $\mathcal{I}^{(0)}$ is the Fisher information of the location parameter provided by *one* real noise sample with distribution $\mathcal{S}(\alpha, 1)$ [34]. A proof is provided in Appendix-A. Given (19) and (20), the optimal detection rule as $N \to \infty$ is

$$\begin{aligned} \acute{\mathbf{x}}_{(1)} &= \underset{\boldsymbol{\zeta}\in\mathbb{S}}{\arg\min}\ \|\bar{\mathbf{H}}(\hat{\mathbf{x}}_{(1)} - \boldsymbol{\zeta})\| \\ &= \underset{\boldsymbol{\zeta}\in\mathbb{S}}{\arg\min} \sum_{k=1}^{K} |\hat{x}_{\ell_k} - \zeta_k|^2, \end{aligned} \tag{21}$$

where $\hat{\mathbf{x}}_{(1)} = [\hat{x}_{\ell_1}, \hat{x}_{\ell_2}, \ldots, \hat{x}_{\ell_K}]^{\mathsf{T}}$ and $\acute{\mathbf{x}}_{(1)} \in \mathbb{S}$ is the hard-estimate of $\mathbf{x}_{(1)}$. Analogous to (12), the minimization in (21) is equivalent to minimizing per-carrier and is therefore computationally easy to perform. As $N$ is finite in practical OFDM systems, (20) may not truly represent the distribution of $\mathbf{e}$. Moreover, as $\alpha$ decreases, the convergence to (20) is *increasingly slower* [32]. Therefore, employing (21) for small $N$ will be suboptimal. However, the reason for generating soft-values in the first place is to allow for low-complexity detection. Also, the solution of (21) offers good error performance for practical values of $\alpha$ and moderately large $N$. This is justified by the BER results in our simulations - see Section IV-C.

In the Gaussian case, the ML estimate of $\mathbf{x}_{(1)}$ is evaluated from (12) by substituting $\boldsymbol{\zeta}$ with $\boldsymbol{\mu} \in \mathbb{C}^K$ and is in analytical form:

$$\begin{aligned} \hat{\mathbf{x}}_{(1)} &= \bar{\mathbf{H}}^{-1}\acute{\mathbf{y}} = \mathbf{x}_{(1)} + \bar{\mathbf{H}}^{-1}\acute{\mathbf{z}} \\ &= \mathbf{x}_{(1)} + \underbrace{\bar{\mathbf{H}}^{-1}\bar{\mathbf{A}}\mathbf{z}}_{\mathbf{e}}. \end{aligned} \tag{22}$$

This is also the *linear least square* solution of (5). From the discussion on (8), $\acute{\mathbf{z}}$ is a Gaussian vector. Therefore,

$$\begin{aligned} \mathbf{e} &\sim \mathcal{CN}(\mathbf{0}_{K\times 1}, E[\mathbf{e}\mathbf{e}^{\mathsf{H}}]) \\ &\sim \mathcal{CN}(\mathbf{0}_{K\times 1}, 4\delta_z^2(\bar{\mathbf{H}}^{\mathsf{H}}\bar{\mathbf{H}})^{-1}) \end{aligned}$$

for *all* $N$. Given (22), one can then employ isotropic (per-carrier) detection via the rule in (21). This overall process is equivalent to the joint-detection rule in (12).

As discussed in Section III, $f_z(\cdot)$ is generally not in closed form. Further still, the cost function in (18) is *not* convex as $f_Z(\cdot) \approx D_{\alpha,\delta_z}|\cdot|^{-\alpha-1}$ at the tails where $D_{\alpha,\delta_z}$ is a positive constant dependent on $\alpha$ and $\delta_z$ [8], [11]. Therefore, solving (18) (even for small $N$) may not be practically feasible. From generalized ML estimation (or M-estimation) theory [35], $f_z(\cdot)$ in (18) is replaced by a more general function $\rho(\cdot) \in \mathbb{R}^+$, i.e.,

$$\begin{aligned} \hat{\mathbf{x}}_{(1)}, \hat{\mathbf{z}} = \quad & \underset{\boldsymbol{\mu},\boldsymbol{\gamma}}{\mathtt{arg\,min}} \quad \textstyle\sum_{n=1}^{N} -\log \rho(\gamma_n) \\ & \mathtt{s.t.} \quad \bar{\mathbf{A}}\mathbf{y} = \bar{\mathbf{H}}\boldsymbol{\mu} + \bar{\mathbf{A}}\boldsymbol{\gamma} \\ & \qquad\quad \bar{\bar{\mathbf{A}}}\mathbf{y} = \bar{\bar{\mathbf{A}}}\boldsymbol{\gamma}. \end{aligned} \tag{23}$$

The relationship in (19) holds for any $\rho(\cdot)$. To achieve near-ML performance, $\rho(\cdot)$ should approximate $f_z(\cdot)$ very well. Though the efficiency of the estimator reduces, choosing a suitable $\rho(\cdot)$ may significantly lessen the computational-cost of evaluating $\hat{\mathbf{x}}_{(1)}$. This is discussed in the next section.

On a final note, to accommodate the pilot symbols in the formulation, one needs to add the additional equalities $\mathbf{A}_{\mathsf{P}}\mathbf{y} = \mathbf{H}_{\mathsf{P}}\mathbf{x}_{\mathsf{P}} + \mathbf{A}_{\mathsf{P}}\boldsymbol{\gamma}$ to (23). Analogous to the constructions of $\bar{\mathbf{A}}$ and $\mathbf{x}_{(1)}$, $\mathbf{A}_{\mathsf{P}}^{\mathsf{H}}$ consists of the columns of $\mathbf{A}^{\mathsf{H}}$ corresponding to the locations of the pilot symbols $\mathbf{x}_{\mathsf{P}}$ in $\mathbf{x}$. Similarly, $\mathbf{H}_{\mathsf{P}}$ is the diagonal submatrix of $\mathbf{H}$ with entries corresponding to the locations of the elements of $\mathbf{x}_{\mathsf{P}}$ in $\mathbf{x}$.

## B. The $L_p$-norm as a Cost Function

In the literature, the $L_p$-norm for $p < 2$ has been used effectively to counter impulsive noise with IID samples [2], [8], [36]. Substituting $-\log \rho(\cdot) = |\Re\{\cdot\}|^p + |\Im\{\cdot\}|^p$ in (23), we get

$$\begin{aligned} \hat{\mathbf{x}}_{(1)}, \hat{\mathbf{z}} = \quad & \underset{\boldsymbol{\mu},\boldsymbol{\gamma}}{\mathtt{arg\,min}} \quad \|\boldsymbol{\gamma}\|_p \\ & \mathtt{s.t.} \quad \bar{\mathbf{A}}\mathbf{y} = \mathbf{H}\boldsymbol{\mu} + \bar{\mathbf{A}}\boldsymbol{\gamma} \\ & \qquad\quad \bar{\bar{\mathbf{A}}}\mathbf{y} = \bar{\bar{\mathbf{A}}}\boldsymbol{\gamma} \end{aligned} \tag{24}$$

where $\|\cdot\|_p$ denotes the $L_p$-norm. The $L_p$-norm for $1 \leq p \leq 2$ is a convex function and may be readily solved via low-complexity numerical techniques [20]. From another perspective, (24) arises from approximating $f_z(\cdot)$ by

$$\begin{aligned} f_z(\cdot) &\approx f_g(\Re\{\cdot\}) f_g(\Im\{\cdot\}) \\ &= C_{p,\delta_z}^2 \exp\left(-\frac{|\Re\{\cdot\}|^p + |\Im\{\cdot\}|^p}{\delta_z^p}\right), \end{aligned} \tag{25}$$

where

$$f_g(x) = C_{p,\delta_z} \exp\left(-\frac{|x|^p}{\delta_z^p}\right) \tag{26}$$

is the zero-mean univariate PDF of a generalized Gaussian distribution (GGD) with scale $\delta_z$, shape parameter $p \in \mathbb{R}^+$ and $C_{p,\delta_z}$ is a positive constant dependent on $p$ and $\delta_z$. The GGD is heavy-tailed for $p < 2$. For $p = 2$, (26) reduces to a Gaussian PDF.

Unlike (18), it is observed that the cost function in (24) is not dependent on $\delta_z$. As the $q^{th}$ order moment of an S$\alpha$S distribution is finite if and only if $q < \alpha$ [8], (24) converges (in the ergodic-sense) to a finite $\hat{\mathbf{x}}_{(1)}$ for $p < \alpha$ for large $N$. For the problem to be simultaneously convex and convergent, $1 \leq p < \alpha$. It is desirable for $p$ to lie within this range. This is justifiable as $\alpha \geq 1.5$ is typically a good fit for practical impulsive noise scenarios [1], [37].

From the discussion in Section II-D, one aspect of $\mathbf{z} \overset{d}{=} \mathbf{z}_{\mathrm{IID}}$ is that the noise realizations are sparse. Drawing insights from compressed sensing (CS) theory [38], [39], the $L_1$-norm recovery of $\mathbf{z}$ given the $N-K$ complex samples $\bar{\bar{\mathbf{A}}}\mathbf{y}$ is

$$\begin{aligned} \hat{\mathbf{z}} = \quad & \underset{\boldsymbol{\gamma}}{\mathtt{arg\,min}} \quad \|\boldsymbol{\gamma}\|_1 \\ & \mathtt{s.t.} \quad \bar{\bar{\mathbf{A}}}\mathbf{y} = \bar{\bar{\mathbf{A}}}\boldsymbol{\gamma}. \end{aligned} \tag{27}$$

Following (27), one can subsequently evaluate the soft-estimate of the OFDM symbol via (19). For the extreme case $K = N$, we note that $\hat{\mathbf{z}} = \mathbf{0}_{N\times 1}$ in (27), and therefore (19) is equivalent to evaluating (22).

We note that (27) is merely (24) (for $p = 1$), but without the pair of equalities: $\bar{\mathbf{A}}\mathbf{y} = \mathbf{H}\boldsymbol{\mu} + \bar{\mathbf{A}}\boldsymbol{\gamma}$. Though both techniques are readily solved via linear programming, the latter has more computational-cost due to the added equality constraints. Further still, CS and $L_1$-norm estimation schemes do not require any information about $\alpha$ and $\delta_z$, and are therefore non-parametric. In terms of performance, one would expect the $L_1$-norm minimization to offer better estimates of $\mathbf{x}_{(1)}$ as (24) contains added information (more equalities) and $\mathbf{z}$ is not *truly* sparse as the probability of any $z_n\ \forall\ n \in \{1, 2, \ldots, N\}$ to be equal to zero is infinitely small. However, our simulations confirmed that both techniques perform *at par* for any $K$ and $N$. This is shown in Section IV-C. The application of CS in OFDM to combat impulsive noise is not a new concept [19]. However, its relationship and performance comparison with respect to the ML detection problem in (9) have not been discussed before.

Though we have highlighted computationally efficient ways of evaluating $\hat{\mathbf{x}}_{(1)}$ via (24) and (27), there is still the problem of detecting the transmitted OFDM symbol. We know that $\mathbf{e}$ in (19) is asymptotically normal if $\hat{\mathbf{x}}_{(1)}$ is the ML estimate of $\mathbf{x}_{(1)}$. If the $L_1$-norm minimization or the CS approach is employed, one would expect $\mathbf{e}$ to be a near-Gaussian vector if $(N-K)/N$ is sufficiently large. We therefore employ the Euclidean detector in (21) to compute BER in the next section.

## C. Performance Analysis

As shown in Section III, ML detection in AWS$\alpha$SN offers a substantial improvement in error performance for OFDM over a single-carrier system. However, it is also important to know how the results of the CS and $L_1$-norm minimization problems compare. Do note that one can directly apply the joint-detection rule in (11) for small $K$ as computational complexity is low. Therefore, we only test the CS or $L_1$-norm minimization approaches when $K$ is sufficiently large.

In Fig. 4, we present the BER performance for $\mathbf{z} \overset{d}{=} \mathbf{z}_{\mathrm{IID}}$ with real and imaginary components for $\alpha = 1.5$ and $N = 32$. The results are plotted for varying null carriers. The percentage of nulls is given by $\frac{N-K}{N} \times 100$. The $L_p$-norm estimation scheme in (24) with $p = 1$ was employed with Euclidean detection. Our simulations further revealed that estimation with the $L_1$-norm and the CS approach in (27) and (19) offers *almost*

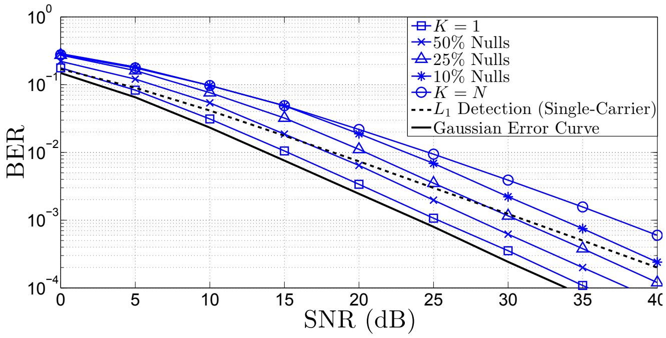


Fig. 4. $L_1$-norm BER performance for BPSK-OFDM averaged over $\bar{\mathbf{H}}$ for $\mathbf{z} \overset{d}{=} \mathbf{z}_{\text{IID}}$ and $\alpha = 1.5$. The curves are generated for $N = 32$.

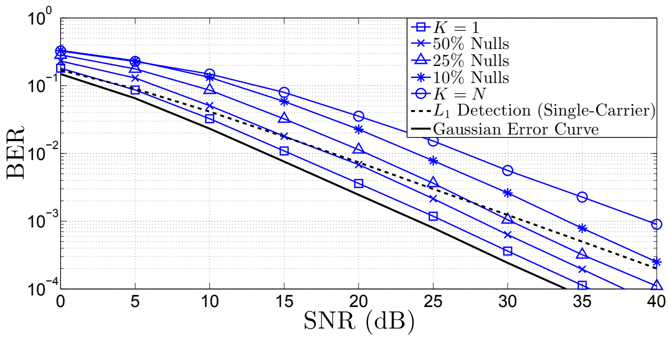


Fig. 5. $L_1$-norm BER performance for BPSK-OFDM averaged over $\bar{\mathbf{H}}$ for $\mathbf{z} \overset{d}{=} \mathbf{z}_{\text{IID}}$ and $\alpha = 1.5$. The curves are generated for $N = 256$.

*similar* performance over a variety of $K$ and $N$ combinations. This is consistent with CS theory [39], as $\mathbf{z}$ is a sparse vector and can be reconstructed very well with a low number of samples (the $N - K$ inequalities in (27)). For clarity, we plot only one BER curve instead of two for each combination of $K$ and $N$. Using the same approach we also plot for $N = 256$ and $N = 512$ in Figs. 5 and 6, respectively, for $\alpha = 1.5$. We note that in all cases, detection performance improves as the number of null carriers increases.

To see the range in which the BER results lie, we plot the best ($K = 1$) and the worst ($K = N$) cases as well. The $K = N$ scenario implies invoking the Euclidean detection rule in (12), while $K = 1$ corresponds to a single-carrier system with $N$ samples. In all plots, we observe that the $K = N$ case worsens as $N$ increases. Also, for 10%, 25% and 50% of null carriers, the BER remains the almost the same irrespective of $N$. For comparison, we have plotted the Gaussian error curve and the BER of a single-carrier system ($K = N = 1$) under $L_1$ detection in all figures.

Though the CS approach makes decoding the OFDM signal feasible, from Figs. 4-6, one can see that a certain number of nulls are required for the system to outperform its single-carrier counterpart. On the contrary, as seen in Fig. 2, ML detection outperforms a single-carrier system even for $K = N$. The trends for the $\alpha = 1.5$ and $\alpha = 1$ cases may be extended intuitively to any $\alpha \neq 2$ as $\mathbf{z}$ is sparse in such scenarios.

The trends seen in Figs. 4-6 also extend to the $\mathbf{z} \overset{d}{=} \mathbf{z}_{\text{ISO}}$ case. This is due to the fact that $\mathbf{z}$ has independent components and

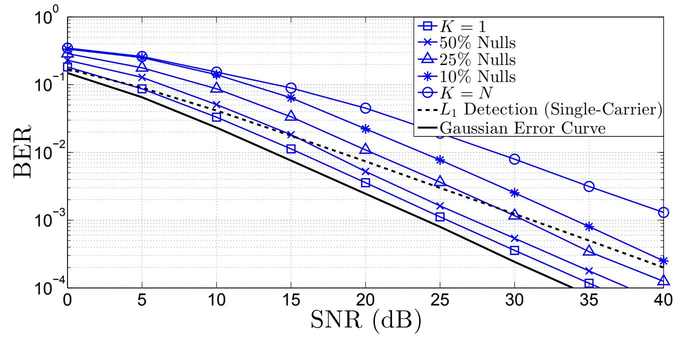


Fig. 6. $L_1$-norm BER performance for BPSK-OFDM averaged over $\bar{\mathbf{H}}$ for $\mathbf{z} \overset{d}{=} \mathbf{z}_{\text{IID}}$ and $\alpha = 1.5$. The curves are generated for $N = 512$.

therefore is sparse for sufficiently large $N$. The solution to (27) also performs well for $\mathbf{z} \overset{d}{=} \mathbf{z}_{\text{ISO}}$ and may be employed.

## V. Receiver Characteristics

Till now we have analyzed computationally-efficient techniques for robust detection of baseband OFDM signals in non-Gaussian AWS$\alpha$SN. In this section, we highlight the design constraints that need to be considered to ensure $\mathbf{z} \overset{d}{=} \mathbf{z}_{\text{IID}}$. We also show that linear passband-to-baseband conversion is actually *sub-optimal* in impulsive noise and reduces the operational SNR of the system. We propose a way around this in Section VI.

### A. Passband-to-Baseband Conversion

The *continuous-time passband* transmit-receive equation for an OFDM signal is given by

$$r(t) = s(t) + w(t) \tag{28}$$

where $r(t)$, $s(t)$ and $w(t)$ are the received signal, the passband OFDM signal and a real AWS$\alpha$SN process, respectively. The relationship of $s(t)$ with its baseband counterpart $\tilde{s}(t)$ is

$$s(t) = \Re\left\{\tilde{s}(t)e^{j2\pi f_c t}\right\} \tag{29}$$

where

$$\tilde{s}(t) = \sum_{k=-N/2}^{N/2-1} \sqrt{\frac{2}{T}} h_k x_k e^{\frac{j2\pi kt}{T}}, \tag{30}$$

$T$ is the time period of the $N$-carrier OFDM symbol block and $f_c$ is the carrier frequency. For simplicity of notation, $N$ is considered to be even. In (5), $x_k$ is the symbol mapped onto the $k^{th}$ sub-carrier $\forall\ k \in \{0, 1, \ldots, N-1\}$. To make this definition consistent with that in (30), we define $x_k = x_l$ and $h_k = h_l$ if $k \equiv l \pmod N$ $\forall\ k, l \in \mathbb{Z}$, i.e., $x_k$ and $h_k$ are periodic with $N$. As before, we assume $K$ data carriers and $N - K$ nulls. Also, the received passband signal energy per-symbol $\mathcal{E}_s$ is related to $\mathcal{E}_x$ as follows

$$\begin{aligned}\mathcal{E}_s = \frac{1}{K}\int_0^T E[|s(t)|^2]\mathrm{d}t &= \frac{1}{2K}\int_0^T E[|\tilde{s}(t)|^2]\mathrm{d}t \\ &= \frac{1}{K}\sum_{k=-N/2}^{N/2-1} E[|h_k|^2]E[|x_k|^2] \\ &= \mathcal{E}_x\sigma_h^2. \end{aligned} \tag{31}$$

The transmitted signal in (5) can be obtained by scaling and sampling $\tilde{s}(t)$. From the properties of the IDFT, we have

$$\begin{aligned}\mathbf{a}_n^{\mathsf{H}}\mathbf{H}\mathbf{x} &= \sum_{k=0}^{N-1}\frac{1}{\sqrt{N}}h_k x_k e^{\frac{j2\pi kn}{N}} \\ &= \sum_{k=-N/2}^{N/2-1}\frac{1}{\sqrt{N}}h_k x_k e^{\frac{j2\pi kn}{N}} \\ &= \sqrt{\frac{T}{2N}}\tilde{s}(nT/N) \end{aligned} \tag{32}$$

$\forall\, n \in \{0,1,\ldots,N-1\}$. To allow downsampling via an integer factor, $T$ should be restricted to a multiple of $N$ and this is therefore implicitly assumed.

To ensure undistorted passband transmission, $f_c$ has to be greater than the largest *absolute* frequency component in (30). This is the sum of $N/(2T)$ (the largest $|k|$ in (30)) and a factor proportional to the bandwidth per-carrier ($1/T$). For simplicity, we choose the factor to be equal to 1. Therefore,

$$f_c > \left(\frac{N}{2}+1\right)\frac{1}{T}. \tag{33}$$

The nulls in $\mathbf{x}$ are typically placed at the ends of the index set $k \in \{-N/2,\ldots,N/2-1\}$ [13]. The bound in (33) can be relaxed depending on the number of nulls. However, it does guarantee undistorted transmission for all possible $K \le N$.

To attain $\mathbf{z} \overset{d}{=} \mathbf{z}_{\text{IID}}$, the passband signal needs to be discretized via a specific sampling rule along with certain constraints [7]. This is a difficult task to do as $f_c$ may be large in practical systems, such as in wireless communications [25]. However, in some impulsive noise scenarios, such as underwater acoustic communications, operational values of $f_c$ are much lower and therefore this approach is feasible [37], [40]. In fact, passband sampling is employed in some underwater modems [37], [40], [41]. We will now further explain these design constraints and extend the results to the $\mathbf{z} \overset{d}{=} \mathbf{z}_{\text{ISO}}$ case.

Denoting the passband sampling frequency by $f_s = \lambda/T$, where $\lambda \in \mathbb{Z}^+$, the discrete-time equation corresponding to (28) can be written as

$$r[n] = s[n] + w[n] \tag{34}$$

$\forall\, n \in \{0,1,\ldots,\lambda-1\}$, where $w[n] \overset{d}{=} W \sim \mathcal{S}(\alpha,\delta_w)$. We use the abridged square bracket notation to denote a discrete signal, i.e., $r[n] = r(n/f_s)$. We also assume that the Nyquist criterion is met. Mathematically, this is given by

$$\begin{aligned} f_s > 2\left(\frac{N}{2T}+f_c\right) &= 2f_c + \frac{N}{T} \\ &\Rightarrow \lambda > 2f_cT + N. \end{aligned} \tag{35}$$

The discretized versions of (29) and (30) are

$$s[n] = \Re\left\{\tilde{s}[n]e^{\frac{j2\pi f_c n}{f_s}}\right\} \tag{36}$$

and

$$\tilde{s}[n] = \sum_{k=-N/2}^{N/2-1}\sqrt{\frac{2f_s}{\lambda}}h_k x_k e^{\frac{j2\pi kn}{\lambda}}, \tag{37}$$

respectively. To get $\tilde{s}[n]$ from $s[n]$, one needs to multiply the latter with a complex exponential, scale by 2 and pass the result through a lowpass filter. Precisely,

$$\tilde{s}[n] = 2v[n] * \left(s[n]e^{-\frac{j2\pi f_c n}{f_s}}\right) \tag{38}$$

where $v[n]\ \forall\ n \in \{0,1,\ldots,L-1\}$ is the $L$-tap impulse response of the lowpass filter and $*$ is the linear convolution operator. Only the in-band information is retained, therefore the effective frequency response of $v[n]$ lies in $[-\frac{N}{2\lambda},\frac{N}{2\lambda}]$. From (32), we have

$$\mathbf{a}_n^{\mathsf{H}}\mathbf{H}\mathbf{x} = \sqrt{\frac{\lambda}{2f_sN}}\tilde{s}[\lambda n/N] \tag{39}$$

$\forall\, n \in \{0,1,\ldots,N-1\}$. To allow downsampling by an integer factor, $\lambda$ needs to be a multiple of $N$, i.e., $\gcd(N,\lambda) = N$. This is implicitly assumed.

### B. Design Constraints

As the passband-to-baseband conversion process is a linear system, analogous to (37) and (39), we get

$$\tilde{w}[n] = 2v[n] * \left(w[n]e^{-\frac{j2\pi f_c n}{f_s}}\right) \tag{40}$$

$\forall\ n \in \{0,1,\ldots,\lambda-1\}$ and

$$z_n = \sqrt{\frac{\lambda}{2f_sN}}\tilde{w}[\lambda n/N] \tag{41}$$

$\forall\ n \in \{0,1,\ldots,N-1\}$, respectively. To ensure $z_n$ has IID real and imaginary components, from (41), it is sufficient to prove that $\tilde{w}[n]$ has IID real and imaginary components. For the latter to hold, the condition $f_s = 4f_c$ *must* be met for $\alpha \neq 2$ [7], [27]. This can be seen by substituting $f_s = 4f_c$ in (40) to get

$$\tilde{w}[n] = 2v[n] * \left(w[n]e^{-\frac{j\pi n}{2}}\right) \tag{42}$$

and observing that

$$\Re\{\tilde{w}[n]\} = 2v[n] * w[n]\cos(\pi n/2) \quad \text{and} \tag{43}$$

$$\Im\{\tilde{w}[n]\} = -2v[n] * w[n]\sin(\pi n/2). \tag{44}$$

As $\cos(\pi n/2)$ is non-zero only when $\sin(\pi n/2) = 0\ \forall\ n \in \mathbb{Z}$ and vice-versa, we note that the real and imaginary components of $\tilde{w}[n]$ are generated from two dissimilar sample sets of $w[n]$. Therefore, $\Re\{\tilde{w}[n]\}$ and $\Im\{\tilde{w}[n]\}$ are mutually *independent* $\forall\ n \in \{0,1,\ldots,N-1\}$. Further still, the expressions in (43) and (44) are *statistically identical* for all $n$. We provide a proof in Appendix-B and show that

$$\Re\{\tilde{w}[n]\} \overset{d}{=} \Im\{\tilde{w}[n] \overset{d}{=} \frac{2}{2^{1/\alpha}}W\left(\sum_{m=0}^{L-1}|v[m]|^{\alpha}\right)^{1/\alpha} \tag{45}$$

for $f_s = 4f_c$. For a more general analysis of the characteristics of baseband noise if $w[n]$ is a non-Gaussian AWS$\alpha$SN process, readers are advised to refer to [7], [27].

Though $f_s = 4f_c$ ensures that the real and imaginary parts of $z_n$ are IID, it does not guarantee independence within the components of $\mathbf{z}$. From (41), a sufficient condition for this to hold is the mutual independence of $\tilde{w}[\lambda n/N]\ \forall\ n \in \{0, 1, \ldots, N-1\}$. As $w[n]$ are samples of an AWS$\alpha$SN process, from (41) we see that the condition is satisfied by constraining $L$ to

$$L \leq \lambda/\gcd(N, \lambda) = \lambda/N. \tag{46}$$

Do note that the filter order and its cutoff both depend on $\lambda/N$.

As discussed in Section II-D, for $\mathbf{z} \overset{d}{=} \mathbf{z}_{\text{ISO}}$, the passband-to-baseband conversion needs to be performed in the continuous-time domain. The $f_s = 4f_c$ constraint does not apply here [7]. However, to attain independence within the components of $\mathbf{z}$ the impulse response $v(t)$ needs to be limited to the time interval $t \in [0, T/N]$. To attain this result, we note that the passband-to-baseband conversion block is a linear system. Therefore, from (32)

$$z_n = \sqrt{\frac{T}{2N}}\tilde{w}(nT/N). \tag{47}$$

Analogous to the relationship between (41) and (46), the constraint on $v(t)$ follows directly from (47).

### C. SNR Degradation

The passband-to-baseband process is sub-optimal in non-Gaussian AWS$\alpha$SN, even for $\mathbf{z} \overset{d}{=} \mathbf{z}_{\text{IID}}$. This is due to the fact that the passband-to-baseband conversion block discussed in Section V-A is optimized for AWGN. As this results in a linear system, the process is sub-optimal in S$\alpha$S noise [8]. This can be quantified as SNR degradation. We can evaluate the distribution of $z_n$ from (2), (41) and (45):

$$\Re\{z_n\} \overset{d}{=} \Im\{z_n\} \overset{d}{=} \frac{1}{2^{1/\alpha}}\sqrt{\frac{2\lambda}{f_s N}}W\left(\sum_{m=0}^{L-1}|v[m]|^\alpha\right)^{1/\alpha} \tag{48}$$

$\forall\ n \in \{0, 1, \ldots, N-1\}$. From (2) and (48) we have

$$\delta_z = \frac{1}{2^{1/\alpha}}\sqrt{\frac{2\lambda}{f_s N}}\delta_w\left(\sum_{m=0}^{L-1}|v[m]|^\alpha\right)^{1/\alpha}. \tag{49}$$

Let $V(f)$ be the discrete-time Fourier transform (DTFT) of $v[n]$. As $V(f)$ is (effectively) non-zero (with unit magnitude) only in the interval $f \in [-\frac{N}{2\lambda}, \frac{N}{2\lambda}]$, we have from Parserval's theorem:

$$\sum_{n=0}^{L-1}|v[n]|^2 = \int_{-1/2}^{1/2}|V(f)|^2\mathrm{d}f \approx \frac{N}{\lambda}$$
$$\Rightarrow \left(\sum_{n=0}^{L-1}|v[n]|^2\right)^{1/2} \approx \sqrt{\frac{N}{\lambda}}. \tag{50}$$

TABLE I
TABULATED VALUES FOR (55).

| | | L: 20 | 40 | 100 | 200 |
|---|---|---|---|---|---|
| $\alpha$ | 1 | 10.0 | 13.0 | 17.0 | 20.0 |
| | 1.2 | 6.7 | 8.7 | 11.3 | 13.3 |
| | 1.4 | 4.3 | 5.6 | 7.3 | 8.6 |
| | 1.6 | 2.5 | 3.3 | 4.2 | 5.0 |
| | 1.8 | 1.1 | 1.4 | 1.9 | 2.2 |

This allows us to express (49) as

$$\delta_z = \frac{1}{\sqrt{f_s}}\delta_w\frac{2^{1/2}\left(\sum_{m=0}^{L-1}|v[m]|^\alpha\right)^{1/\alpha}}{2^{1/\alpha}\left(\sum_{m=0}^{L-1}|v[m]|^2\right)^{1/2}} \tag{51}$$

or from (82) and (84) (in Appendix-B),

$$\delta_z = \frac{1}{\sqrt{f_s}}\delta_w\frac{\left(\sum_{m=0}^{\lfloor\frac{L-1}{2}\rfloor}|v[2m]|^\alpha\right)^{1/\alpha}}{\left(\sum_{m=0}^{\lfloor\frac{L-1}{2}\rfloor}|v[2m]|^2\right)^{1/2}}. \tag{52}$$

Defining $\tilde{\mathbf{v}} = [v_1, v_2, \ldots, v_{\lfloor\frac{L+1}{2}\rfloor}]^\mathsf{T}$ such that $v_{m+1} = v[2m]\ \forall\ m \in \{0, 1, \ldots, \lfloor\frac{L-1}{2}\rfloor\}$, we have

$$\delta_z = \frac{1}{\sqrt{f_s}}\delta_w\frac{\|\tilde{\mathbf{v}}\|_\alpha}{\|\tilde{\mathbf{v}}\|_2}. \tag{53}$$

Substituting this back into (13), we get

$$\text{SNR}_{\text{dB}} = 10\log_{10}\frac{\mathcal{E}_x\sigma_h^2 f_s}{4\delta_w^2\log_2 M} - 20\log_{10}\frac{\|\tilde{\mathbf{v}}\|_\alpha}{\|\tilde{\mathbf{v}}\|_2}. \tag{54}$$

As $4\delta_w^2/f_s = N_0$ for the Gaussian case, we term $4\delta_w^2/f_s$ as the *pseudo*-PSD of the passband AWS$\alpha$SN process.

For a given pseudo-PSD, the SNR depends on $v[n]$, $\alpha$ and $L$. As $\|\tilde{\mathbf{v}}\|_\alpha \geq \|\tilde{\mathbf{v}}\|_2$ for any $\tilde{\mathbf{v}} \in \mathbb{R}^{\lfloor\frac{L+1}{2}\rfloor}$, the latter term in (54) is always positive and therefore causes reduction in the SNR. To visualize this effect, let $v[n] = \frac{1}{L}\ \forall\ n \in \{0, 1, \ldots, L-1\}$, i.e., it computes the average of the samples that fall into the convolution window. This results in

$$20\log_{10}\frac{\|\tilde{\mathbf{v}}\|_\alpha}{\|\tilde{\mathbf{v}}\|_2} = 10\left(\frac{2}{\alpha} - 1\right)\log_{10}\left\lfloor\frac{L+1}{2}\right\rfloor. \tag{55}$$

We see that the SNR degradation varies logarithmically with $\lfloor\frac{L+1}{2}\rfloor$ and linearly with $2/\alpha - 1$. In Table I, we have listed outcomes of (55) for various $\alpha$ and $L$. Even for $\alpha$ close to 2, there is at least a loss of 1 dB. On a final note, we observe that for $\alpha = 2$, the latter term in (54) is equal to zero for any $\tilde{\mathbf{v}}$. This signifies that the SNR depends only on the signal and noise powers in AWGN [25].

## VI. PASSBAND ESTIMATION AND DETECTION

Instead of conversion to baseband, we can estimate soft-values of $\mathbf{x}_{(1)}$ directly from the passband samples. By doing so, we can avoid the SNR loss in passband-to-baseband conversion. Further still, the constraints that induce sparsity in $\mathbf{z}$ (discussed in Section V-B) do not need to be enforced if the passband samples are processed directly.

We define $x_k = x_l$ and $h_k = h_l$ if $k \equiv l \pmod{\lambda}$, i.e., $h_k$ and $x_k$ are periodic in $k$ with sample period $\lambda$. Like before, there are $K$ data-carriers but now with $\lambda - K$ null-carriers. We fix the data location set $\mathcal{L}_{\mathbf{x}}$ to $\{-K/2, \ldots, K/2-1\}$ and $f_c = \xi/T$ where $\xi \in \mathbb{Z}^+$. From (36), (37) and the properties of the IDFT

$$\begin{aligned} s[n] &= \Re\left\{\sqrt{\frac{2f_s}{\lambda}} \sum_{k=-K/2}^{K/2-1} h_k x_k e^{\frac{j2\pi(k+\xi)n}{\lambda}}\right\} \\ &= \Re\left\{\sqrt{\frac{2f_s}{\lambda}} \sum_{k=-\lambda/2}^{\lambda/2-1} h_k x_k e^{\frac{j2\pi(k+\xi)n}{\lambda}}\right\} \\ &= \Re\left\{\sqrt{\frac{2f_s}{\lambda}} \sum_{k=0}^{\lambda-1} h_k x_k e^{\frac{j2\pi(k+\xi)n}{\lambda}}\right\}. \end{aligned} \tag{56}$$

On applying a change of variables from $k+\xi$ to $k$ in (56), we have

$$s[n] = \Re\left\{\sqrt{\frac{2f_s}{\lambda}} \sum_{k=0}^{\lambda-1} h_{k-\xi} x_{k-\xi} e^{\frac{j2\pi kn}{\lambda}}\right\}. \tag{57}$$

As $x_k$, $h_k$ and $e^{\frac{j2\pi kn}{\lambda}}$ are periodic in $k$,

$$\begin{aligned} \sum_{k=0}^{\lambda-1} h^*_{k-\xi} x^*_{k-\xi} e^{-\frac{j2\pi kn}{\lambda}} &= \sum_{k=0}^{\lambda-1} h^*_{k-\xi} x^*_{k-\xi} e^{\frac{j2\pi(\lambda-k)n}{\lambda}} \\ &= \sum_{k=0}^{\lambda-1} h^*_{\lambda-k-\xi} x^*_{\lambda-k-\xi} e^{\frac{j2\pi kn}{\lambda}}. \end{aligned} \tag{58}$$

Using (58), we can express (57) as

$$\begin{aligned} s[n] &= \sqrt{\frac{f_s}{2\lambda}} \sum_{k=0}^{\lambda-1} \left(h_{k-\xi} x_{k-\xi} e^{\frac{j2\pi kn}{\lambda}} + h^*_{k-\xi} x^*_{k-\xi} e^{-\frac{j2\pi kn}{\lambda}}\right) \\ &= \sqrt{\frac{f_s}{2\lambda}} \sum_{k=0}^{\lambda-1} \left(h_{k-\xi} x_{k-\xi} + h^*_{\lambda-k-\xi} x^*_{\lambda-k-\xi}\right) e^{\frac{j2\pi kn}{\lambda}}. \end{aligned} \tag{59}$$

Let $\mathbf{D}$ be the anti-diagonal $\lambda \times \lambda$ matrix with all non-zero elements equal to one. Defining the block diagonal matrix

$$\mathbf{H}_\lambda = \begin{bmatrix} \mathbf{0}_{\xi-\frac{K}{2}} & 0 & \cdots & & 0 \\ 0 & \bar{\mathbf{H}} & \cdots & & 0 \\ \vdots & & \mathbf{0}_{\lambda-2\xi-K+1} & & \vdots \\ & & & \mathbf{D}\bar{\mathbf{H}}^*\mathbf{D} & \\ 0 & & \cdots & & \mathbf{0}_{\xi-\frac{K}{2}-1} \end{bmatrix} \tag{60}$$

and the $\lambda \times 1$ vector

$$\mathbf{x}_\lambda = \begin{bmatrix} \mathbf{0}_{(\xi-\frac{K}{2})\times 1} \\ \mathbf{x}_{(1)} \\ \mathbf{0}_{(\lambda-2\xi-K+1)\times 1} \\ \mathbf{D}\mathbf{x}^*_{(1)} \\ \mathbf{0}_{(\xi-\frac{K}{2}-1)\times 1} \end{bmatrix}, \tag{61}$$

we can represent (59) in the following vector form:

$$\mathbf{s} = \sqrt{\frac{f_s}{2}} \mathbf{A}_\lambda^{\mathsf{H}} \mathbf{H}_\lambda \mathbf{x}_\lambda. \tag{62}$$

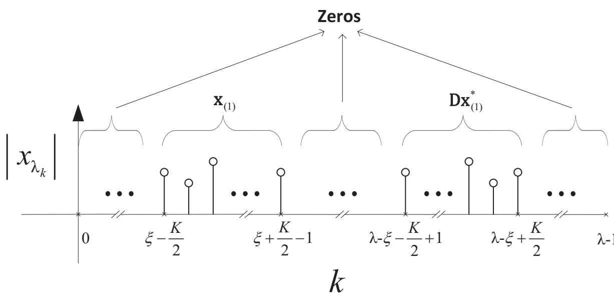


Fig. 7. Placement of symbols and nulls in $\mathbf{x}_\lambda$.

Here $\mathbf{A}_\lambda$ is the *unitary* $\lambda$-point DFT matrix. Though $\mathbf{H}_\lambda$ and $\mathbf{x}_\lambda$ are complex, do note that $\mathbf{s} \in \mathbb{R}^\lambda$. Finally, using (62) we have

$$\mathbf{r} = \sqrt{\frac{f_s}{2}} \mathbf{A}_\lambda^{\mathsf{H}} \mathbf{H}_\lambda \mathbf{x}_\lambda + \mathbf{w}, \tag{63}$$

where $r[n]$ and $w[n]$ $\forall\ n \in \{0, 1, \ldots, \lambda-1\}$ in (34) are the $(n+1)^{th}$ elements of $\mathbf{r}$ and $\mathbf{w}$, respectively. The problem in (63) is similar to that in (5). The difference lies in the inherent structure of $\mathbf{H}_\lambda$ and $\mathbf{x}_\lambda$. We also note that $\mathbf{r}, \mathbf{w} \in \mathbb{R}^\lambda$. Denoting the elements of $\mathbf{x}_\lambda$ by the $\lambda$-tuple $[x_{\lambda_0}, x_{\lambda_1}, \ldots, x_{\lambda_{\lambda-1}}]^{\mathsf{T}}$, we plot $|x_{\lambda_k}|$ against $k$ in Fig. 7 for added clarity. From Fig. 7, we see that the constraints

$$\xi \geq \frac{K}{2} + 1 \quad \text{and} \quad \lambda \geq 2\xi + K, \tag{64}$$

ensure that the sidebands do not overlap and therefore need to be enforced to guarantee non-lossy transmission.

Analogous to (27), the CS estimate of $\mathbf{w}$ is given by

$$\begin{aligned} \hat{\mathbf{w}} = \quad & \underset{\boldsymbol{\gamma}\in\mathbb{R}^\lambda}{\texttt{arg min}} \quad \|\boldsymbol{\gamma}\|_1 \\ & \texttt{s.t.} \quad\quad \bar{\bar{\mathbf{A}}}_\lambda \mathbf{r} = \bar{\bar{\mathbf{A}}}_\lambda \boldsymbol{\gamma}. \end{aligned} \tag{65}$$

where $\bar{\bar{\mathbf{A}}}_\lambda \in \mathbb{C}^{(\lambda-2K)\times\lambda}$ consists of the columns of $\mathbf{A}^*_\lambda$ corresponding to the locations of nulls in $\mathbf{x}_\lambda$. Given $\hat{\mathbf{w}}$, a modified passband equation may be constructed from (63)

$$\tilde{\mathbf{r}} = \sqrt{\frac{f_s}{2}} \mathbf{A}_\lambda^{\mathsf{H}} \mathbf{H}_\lambda \mathbf{x}_\lambda + (\mathbf{w} - \hat{\mathbf{w}}). \tag{66}$$

If $\lambda - 2K$ is greater than a certain threshold, the recovery of $\mathbf{w}$ via (65) will be good. Typically, $\lambda - 2K$ will be of large value. Following a similar line of reasoning as in (20), $\mathbf{w} - \hat{\mathbf{w}}$ can be well approximated by a Gaussian distribution with IID components. Thereafter, $\tilde{\mathbf{r}}$ may be passed through a linear passband-to-baseband conversion block to construct (5) with isotropic Gaussian $\mathbf{z}$. The ML detector in (12) may then be subsequently employed to generate hard-estimates of the transmitted symbols. Alternatively, (66) can be normalized by $\sqrt{\frac{f_s}{2}}$ and left-multiplied by $\mathbf{H}_\lambda^{-1}\mathbf{A}_\lambda$ to form

$$\acute{\mathbf{r}} = \mathbf{H}_\lambda \mathbf{x}_\lambda + \acute{\mathbf{e}} \tag{67}$$

where $\acute{\mathbf{r}} = \sqrt{\frac{2}{f_s}} \mathbf{A}_\lambda \tilde{\mathbf{r}}$ and $\acute{\mathbf{e}} = \sqrt{\frac{2}{f_s}} \mathbf{A}_\lambda (\mathbf{w} - \hat{\mathbf{w}})$. Do note that $\acute{\mathbf{e}} \in \mathbb{C}^\lambda$ is approximately Gaussian as it is a linear

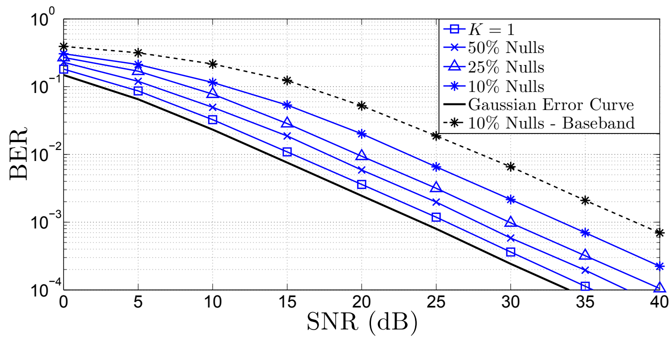


Fig. 8. $L_1$-norm BER performance for BPSK-OFDM averaged over $\bar{\mathbf{H}}$ for $\alpha = 1.5$. The curves are generated for $\lambda = 256$ and decoding was performed directly on the passband samples.

transformation of $\mathbf{w} - \hat{\mathbf{w}}$. Further still, $\acute{\mathbf{e}}$ has IID components due to the orthonormal columns of $\mathbf{A}_\lambda$. Precisely, $\acute{\mathbf{e}} \sim \mathcal{CN}(\mathbf{0}_{\lambda\times 1}, 2\delta_{\acute{e}}^2\mathbf{I}_\lambda)$, where $2\delta_{\acute{e}}^2$ is the variance of each component of $\acute{\mathbf{e}}$. Therefore, we can remove the nulls and express (67) in terms of $\mathbf{x}_{(1)}$ and the corresponding received components:

$$\begin{bmatrix}\acute{\mathbf{r}}_1\\ \acute{\mathbf{r}}_2\end{bmatrix} = \begin{bmatrix}\bar{\mathbf{H}}\mathbf{x}_{(1)}\\ \mathbf{D}\bar{\mathbf{H}}^*\mathbf{x}^*_{(1)}\end{bmatrix} + \begin{bmatrix}\acute{\mathbf{e}}_1\\ \acute{\mathbf{e}}_2\end{bmatrix}, \qquad (68)$$

where $\acute{\mathbf{r}}_1, \acute{\mathbf{r}}_2, \acute{\mathbf{e}}_1, \acute{\mathbf{e}}_2 \in \mathbb{C}^K$. Finally, the soft-estimate of $\mathbf{x}_{(1)}$ can be evaluated as

$$\begin{aligned}\hat{\mathbf{x}}_{(1)} &= \bar{\mathbf{H}}^{-1}\frac{\acute{\mathbf{r}}_1 + \mathbf{D}\acute{\mathbf{r}}_2^*}{2}\\ &= \mathbf{x}_{(1)} + \underbrace{\bar{\mathbf{H}}^{-1}\frac{\acute{\mathbf{e}}_1 + \mathbf{D}\acute{\mathbf{e}}_2^*}{2}}_{\mathbf{e}},\end{aligned} \qquad (69)$$

where $\mathbf{e} \sim \mathcal{CN}(\mathbf{0}_{K\times 1}, 2\delta_{\acute{e}}^2(\bar{\mathbf{H}}^{\mathsf{H}}\bar{\mathbf{H}})^{-1})$. This will be followed by the ML detection rule in (21).

In contrast to the baseband approach, there have been no assumptions about the relationship between $f_c$ and $f_s$. Further still, by performing operations in the passband, there is no SNR degradation due to linear passband-to-baseband conversion. Also, as $\lambda$ is typically greater than $2K$, the CS algorithm will have more samples to work with and therefore $\mathbf{w}$ will always be a good estimate. On the downside, passband sampling is difficult to perform when $f_c$ is large. This is compounded by the fact that as $\lambda$ increases, the DFT and CS operations increase in complexity as well.

To sum up our discussion, we present the BER performance of BPSK-OFDM for $\lambda = 256$ and $\alpha = 1.5$ with varying nulls in Fig. 8. The trends are similar to those encountered in Fig. 5. If the measure in (54) is used, then the BER performance may be *increased* arbitrarily over its baseband counterpart by varying $\tilde{\mathbf{v}}$. Therefore, we employ the following SNR definition:

$$\mathrm{SNR_{dB}} = 10\log_{10}\frac{\mathcal{E}_x\sigma_h^2 f_s}{4\delta_w^2\log_2 M}. \qquad (70)$$

To highlight the increase in performance over a system that employs baseband conversion, we also plot the BER for the latter in Fig. 8 for $N = 256$ and 10% nulls for $\alpha = 1.5$. We employ a 40-tap low pass filter with impulse response $v[n] = \frac{1}{40}\ \forall\ n \in \{0, 1, \ldots, 39\}$. From (55), the loss in SNR due to baseband conversion is approximately 4.3 dB. The advantage of passband processing can be clearly appreciated in Fig. 8.

## VII. Conclusions

This paper highlights receiver design for OFDM signaling in a Rayleigh block-fading channel contaminated with AWS$\alpha$SN. In the recent years CS theory has garnered much attention. One of its potential applications lies in the estimation and removal of impulses within an impulsive noise process as the latter is sparse. We have discussed the pros and cons of this approach for OFDM in AWS$\alpha$SN and compare the BER performance with recently discovered ML detection results. The constraints within a linear passband-to-baseband conversion block that guarantee sparsity for baseband noise are also discussed. It is shown that linear passband-to-baseband conversion causes SNR degradation in non-Gaussian AWS$\alpha$SN. We have proposed a way around this by directly processing the passband samples. On a final note, our derivations and simulations assume that the receiver has perfect knowledge of the channel. Consequently, the accuracy of these results depends on the channel estimation scheme adopted at the receiver.

## Appendix

### A. *Proof of* (20)

Let us define

$$\breve{\mathbf{y}} = \begin{bmatrix}\Re\{\mathbf{y}\}\\ \Im\{\mathbf{y}\}\end{bmatrix}, \breve{\mathbf{x}} = \begin{bmatrix}\Re\{\mathbf{x}_{(1)}\}\\ \Im\{\mathbf{x}_{(1)}\}\end{bmatrix} \text{ and } \breve{\mathbf{e}} = \begin{bmatrix}\Re\{\mathbf{e}\}\\ \Im\{\mathbf{e}\}\end{bmatrix}. \qquad (71)$$

Do note that $\breve{\mathbf{y}}, \breve{\mathbf{x}}, \breve{\mathbf{e}} \in \mathbb{R}^{2K}$. We can express (6) in terms of $\breve{\mathbf{y}}$ and $\breve{\mathbf{x}}$:

$$\breve{\mathbf{y}} = \breve{\mathbf{A}}^{\mathsf{T}}\breve{\mathbf{H}}\breve{\mathbf{x}} + \breve{\mathbf{z}} \qquad (72)$$

where

$$\breve{\mathbf{A}} = \begin{bmatrix}\Re\{\bar{\mathbf{A}}\} & -\Im\{\bar{\mathbf{A}}\}\\ \Im\{\bar{\mathbf{A}}\} & \Re\{\bar{\mathbf{A}}\}\end{bmatrix}, \ \breve{\mathbf{H}} = \begin{bmatrix}\Re\{\bar{\mathbf{H}}\} & -\Im\{\bar{\mathbf{H}}\}\\ \Im\{\bar{\mathbf{H}}\} & \Re\{\bar{\mathbf{H}}\}\end{bmatrix}$$

and

$$\breve{\mathbf{z}} = \begin{bmatrix}\Re\{\mathbf{z}\}\\ \Im\{\mathbf{z}\}\end{bmatrix}.$$

In (19), if $\hat{\mathbf{x}}_{(1)}$ is the ML estimate of $\mathbf{x}_{(1)}$, then from the asymptotic normality of ML estimation,

$$\breve{\mathbf{e}} \sim \mathcal{N}(\mathbf{0}_{2K\times 1}, \mathbf{\Sigma}^{-1}) \qquad (73)$$

as $N \to \infty$. Here $\mathbf{\Sigma}$ is the Fisher information matrix of $\breve{\mathbf{x}}$ with respect to the distribution $\tilde{f}(\mathbf{y}; \breve{\mathbf{x}}) = f_{\mathbf{z}}(\mathbf{y} - \bar{\mathbf{A}}^{\mathsf{H}}\bar{\mathbf{H}}\mathbf{x}_{(1)})$ [32]. Further still, as the model in (6) is that of linear regression, we have from [34], [42, Eq. 58]

$$\begin{aligned}\mathbf{\Sigma} &= \frac{\mathcal{I}^{(0)}}{\delta_z^2}(\breve{\mathbf{A}}^{\mathsf{T}}\breve{\mathbf{H}})^{\mathsf{T}}\breve{\mathbf{A}}^{\mathsf{T}}\breve{\mathbf{H}}\\ &= \frac{\mathcal{I}^{(0)}}{\delta_z^2}\breve{\mathbf{H}}^{\mathsf{T}}\breve{\mathbf{A}}\breve{\mathbf{A}}^{\mathsf{T}}\breve{\mathbf{H}} = \frac{\mathcal{I}^{(0)}}{\delta_z^2}\breve{\mathbf{H}}^{\mathsf{T}}\breve{\mathbf{H}},\end{aligned} \qquad (74)$$

where $\mathcal{I}^{(0)}$ is the Fisher information of the location parameter provided by *one* real noise sample with distribution $\mathcal{S}(\alpha, 1)$ [34]. On substituting (74) into (73), we have

$$\breve{\mathbf{e}} \sim \mathcal{N}(\mathbf{0}_{2K\times 1}, \frac{\delta_z^2}{\mathcal{I}^{(0)}}(\breve{\mathbf{H}}^{\mathsf{T}}\breve{\mathbf{H}})^{-1}). \tag{75}$$

As

$$\breve{\mathbf{H}}^{\mathsf{T}}\breve{\mathbf{H}} = \begin{bmatrix} \bar{\mathbf{H}}^{\mathsf{H}}\bar{\mathbf{H}} & \mathbf{0}_{K\times K} \\ \mathbf{0}_{K\times K} & \bar{\mathbf{H}}^{\mathsf{H}}\bar{\mathbf{H}} \end{bmatrix} \tag{76}$$

is a diagonal matrix, we can clearly see that the elements of $\breve{\mathbf{e}}$ are independent. Finally, taking advantage of the form in (76) and the fact that $\mathbf{e} = [\mathbf{I}_K \quad j\mathbf{I}_K]\breve{\mathbf{e}}$, we have

$$\mathbf{e} \sim \mathcal{CN}(\mathbf{0}_{K\times 1}, \frac{2\delta_z^2}{\mathcal{I}^{(0)}}(\bar{\mathbf{H}}^{\mathsf{H}}\bar{\mathbf{H}})^{-1}). \tag{77}$$

### *B. Proof:* (43) *and* (44) *are statistically identical for all* $n$

The convolution operation in (43) can be written in its true form:

$$\Re\{\tilde{w}[n]\} = 2\sum_{l=0}^{L-1} v[l]w[n-l]\cos(\pi(n-l)/2). \tag{78}$$

As $w[n] \overset{d}{=} W \sim \mathcal{S}(\alpha, \delta_w)$, we can use (1) to express (78) as

$$\Re\{\tilde{w}[n]\} \overset{d}{=} 2W\left(\sum_{l=0}^{L-1} |v[l]\cos(\pi(n-l)/2)|^\alpha\right)^{1/\alpha}. \tag{79}$$

We know that $\cos(\pi(n-l)/2)$ is non-zero only for $l = 2m$ when $n$ is even and $l = 2m+1$ when $n$ is odd, where $m \in \mathbb{Z}$. Further still, the result will lie in the set $\{-1, +1\}$. As symmetric distributions are not influenced by the sign, we have

$$\Re\{\tilde{w}[n]\} \overset{d}{=} 2W\left(\sum_{m=0}^{\lfloor\frac{L-1}{2}\rfloor} |v[2m]|^\alpha\right)^{1/\alpha} \tag{80}$$

when $n$ is even and

$$\Re\{\tilde{w}[n]\} \overset{d}{=} 2W\left(\sum_{m=0}^{\lfloor\frac{L}{2}\rfloor-1} |v[2m+1]|^\alpha\right)^{1/\alpha} \tag{81}$$

when $n$ is odd. The expressions in (80) and (81) depend on the sums of the even and odd samples of $|v[n]|^\alpha$, respectively. We know that $v[n]$ is *effectively* band-limited to $[-\frac{N}{2\lambda}, \frac{N}{2\lambda}]$. Denoting the discrete-time Fourier transform (DTFT) of $|v[n]|^\alpha$ by $V_\alpha(f)$, we note that $V_\alpha(f)$ still retains characteristics of a lowpass filter, i.e., *most* of the energy of $|v[n]|^\alpha$ occupies the lower spectrum for finite $L$ [7]. From the properties of the DTFT,

$$\begin{aligned} V_\alpha(0) &= \sum_{m=0}^{L-1} |v[m]|^\alpha & (82)\\ &= \sum_{m=0}^{\lfloor\frac{L-1}{2}\rfloor} |v[2m]|^\alpha + \sum_{m=0}^{\lfloor\frac{L}{2}\rfloor-1} |v[2m+1]|^\alpha. & (83) \end{aligned}$$

If $V_\alpha(f/2)$ is *truly* band-limited, the energy is divided equally amongst the two summation terms in (83). Therefore,

$$\frac{1}{2}V_\alpha(0) = \sum_{m=0}^{\lfloor\frac{L-1}{2}\rfloor} |v[2m]|^\alpha = \sum_{m=0}^{\lfloor\frac{L}{2}\rfloor-1} |v[2m+1]|^\alpha. \tag{84}$$

In practical filters, $L$ is finite and therefore $V_\alpha(f/2)$ is not truly band-limited. However, (84) provides a good approximation for a large range of $L$ as long as $\lambda$ is at least a few multiples of $N$. Therefore, from (82) and (84), we can express (80) and (81) as

$$\begin{aligned} \Re\{\tilde{w}[n]\} &\overset{d}{=} 2W \times \left(\frac{1}{2}V_\alpha(0)\right)^{1/\alpha} \\ &\overset{d}{=} \frac{2}{2^{1/\alpha}}W\left(\sum_{m=0}^{L-1} |v[m]|^\alpha\right)^{1/\alpha}. & (85) \end{aligned}$$

Using a similar approach as in (78)-(85) we can evaluate the distribution of $\Im\{\tilde{w}[n]\}$ and observe that

$$\Re\{\tilde{w}[n]\} \overset{d}{=} \Im\{\tilde{w}[n]\}. \tag{86}$$

We note from (85) and (86), that the distribution of $\tilde{w}[n]$ is independent of $n$ and therefore time-invariant.

## References

[1] M. Chitre, J. Potter, and S.-H. Ong, "Optimal and near-optimal signal detection in snapping shrimp dominated ambient noise," *IEEE J. Ocean. Eng.*, vol. 31, no. 2, pp. 497 –503, April 2006.

[2] M. Chitre, J. Potter, and S. Ong, "Viterbi decoding of convolutional codes in symmetric $\alpha$-stable noise," *IEEE Commun. Lett.*, vol. 55, no. 12, pp. 2230 –2233, Dec. 2007.

[3] M. Zimmermann and K. Dostert, "Analysis and modeling of impulsive noise in broad-band powerline communications," *IEEE Trans. Energy Convers.*, vol. 44, no. 1, pp. 249 –258, Feb 2002.

[4] M. Nassar, K. Gulati, Y. Mortazavi, and B. Evans, "Statistical modeling of asynchronous impulsive noise in powerline communication networks," in *IEEE Global Telecommunications Conf. (GLOBECOM)*, 2011, pp. 1–6.

[5] T. Al-Naffouri, A. Quadeer, and G. Caire, "Impulsive noise estimation and cancellation in dsl using orthogonal clustering," in *IEEE Int. Symp. on Info. Theory, (ISIT)*, 2011, pp. 2841–2845.

[6] T. Al-Naffouri, A. Quadeer, F. Al-Shaalan, and H. Hmida, "Impulsive noise estimation and cancellation in dsl using compressive sampling," in *IEEE Int. Symp. on Circuits and Systems (ISCAS)*, 2011, pp. 2133–2136.

[7] A. Mahmood, M. Chitre, and M. A. Armand, "PSK communication with passband additive symmetric $\alpha$-stable noise," *IEEE Trans. Commun.*, vol. 60, no. 10, pp. 2990 –3000, Oct. 2012.

[8] C. L. Nikias and M. Shao, *Signal processing with Alpha-Stable Distributions and Applications*. New York: Chapman-Hall, 1996.

[9] D. Middleton, "Non-Gaussian noise models in signal processing for telecommunications: new methods and results for class A and class B noise models," *IEEE Trans. Inf. Theory*, vol. 45, no. 4, pp. 1129–1149, May 1999.

[10] M. Ghosh, "Analysis of the effect of impulse noise on multicarrier and single carrier QAM systems," *IEEE Trans. Commun.*, vol. 44, no. 2, pp. 145–147, Feb. 1996.

[11] G. Samorodnitsky and M. S. Taqqu, *Stable Non-Gaussian Random Processes: Stochastic Models with Infinite Variance*. Chapman & Hall, 1994.

[12] J. P. Nolan, *Stable Distributions - Models for Heavy Tailed Data*. Boston: Birkhauser, 2012, in progress, Chapter 1 online at academic2.american.edu/∼jpnolan.

[13] H. Schulze and C. Lueders, *Theory and Applications of OFDM and CDMA: Wideband Wireless Communications*. Wiley, 2005.

[14] A. Mahmood, M. Chitre, and M. A. Armand, "Maximum-likelihood detection performance of uncoded OFDM in impulsive noise," in *IEEE Global Telecommunications Conf. (GLOBECOM)*, Dec. 2013.

[15] S. Zhidkov, "Analysis and comparison of several simple impulsive noise mitigation schemes for ofdm receivers," *IEEE Trans. Commun.*, vol. 56, no. 1, pp. 5–9, 2008.

[16] K. M. Rabie and E. Alsusa, "Improving blanking/clipping based impulsive noise mitigation over powerline channels," in *Personal Indoor and Mobile Radio Communications (PIMRC), 2013 IEEE 24th Int. Symp. on*, 2013, pp. 3413–3417.

[17] F. Abdelkefi, P. Duhamel, and F. Alberge, "Impulsive noise cancellation in multicarrier transmission," *IEEE Trans. Commun.*, vol. 53, no. 1, pp. 94–106, Jan. 2005.

[18] ——, "A necessary condition on the location of pilot tones for maximizing the correction capacity in OFDM systems," *IEEE Trans. Commun.*, vol. 55, no. 2, pp. 356–366, Feb. 2007.

[19] G. Caire, T. Al-Naffouri, and A. Narayanan, "Impulse noise cancellation in OFDM: an application of compressed sensing," in *IEEE Int. Symp. on Info. Theory, (ISIT)*, July, pp. 1293–1297.

[20] S. Boyd and L. Vandenberghe, *Convex Optimization*. New York, NY, USA: Cambridge Univ. Press, 2004.

[21] J. H. McCulloch, *Numerical approximation of the symmetric stable distribution and density*. Cambridge, MA, USA: Birkhauser Boston Inc., 1998, pp. 489–499.

[22] J. P. Nolan, "Numerical calculation of stable densities and distribution functions," *Communications in Stat. Stochastic Models*, vol. 13, no. 4, pp. 759–774, 1997.

[23] A. Papoulis and U. S. Pillai, *Probability, Random Variables and Stochastic Processes*. Boston: McGraw-Hill, Dec 2001.

[24] A. Goldsmith, *Wireless communications*. Cambridge university press, 2005.

[25] J. Proakis and M. Salehi, *Digital Communications*, ser. McGraw-Hill higher education. McGraw-Hill Education, 2007.

[26] G. Strang, *Linear Algebra and Its Applications*. Thomson Brooks/Cole Cengage learning, 2006.

[27] A. Mahmood, M. Chitre, and M. A. Armand, "Improving PSK performance in snapping shrimp noise with rotated constellations," in *Proc. of the Seventh ACM Int. Conf. on Underwater Networks and Systems*, ser. WUWNet '12, no. 12, New York, NY, USA, 2012, pp. 1–8.

[28] J. G. Gonzalez, "Robust techniques for wireless communications in non-gaussian environments," Ph.D. dissertation, Univ. of Delaware, Newark, DE, USA, 1997.

[29] A. Rajan and C. Tepedelenlioglu, "Diversity combining over rayleigh fading channels with symmetric alpha-stable noise," *IEEE Trans. Wireless Commun.*, vol. 9, no. 9, pp. 2968–2976, 2010.

[30] W. H. DuMouchel, "On the Asymptotic Normality of the Maximum-Likelihood Estimate when Sampling from a Stable Distribution," *The Ann. of Stat.*, vol. 1, no. 5, 1973.

[31] ——, "Stable distributions in statistical inference: 2. information from stably distributed samples," *J. of the American Statistical Assoc.*, vol. 70, no. 350, pp. pp. 386–393, 1975.

[32] J. Nolan, "Maximum likelihood estimation and diagnostics for stable distributions," in *Lvy Processes*, O. Barndorff-Nielsen, S. Resnick, and T. Mikosch, Eds. Birkhuser Boston, 2001, pp. 379–400. [Online]. Available: http://dx.doi.org/10.1007/978-1-4612-0197-7_17

[33] S. Kay, *Fundamentals of Statistical Signal Processing: Estimation Theory*, ser. Fundamentals of Statistical Signal Processing. Prentice-Hall PTR, 1998, no. v. 1.

[34] J. P. Nolan and D. Ojeda-Revah, "Linear and nonlinear regression with stable errors," *J. of Econometrics*, vol. 172, no. 2, pp. 186 – 194, 2013.

[35] P. Huber and E. Ronchetti, *Robust Statistics*, ser. Wiley Series in Probability and Statistics. John Wiley & Sons, Inc., 2009.

[36] E. E. Kuruoglu, P. J. Rayner, and W. J. Fitzgerald, "Least Lp-norm impulsive noise cancellation with polynomial filters," *Signal Processing*, vol. 69, no. 1, pp. 1 – 14, 1998.

[37] M. Chitre, J. Potter, and O. S. Heng, "Underwater acoustic channel characterisation for medium-range shallow water communications," in *OCEANS '04. MTTS/IEEE TECHNO-OCEAN '04*, vol. 1, Nov. 2004, pp. 40 –45.

[38] E. Candes and P. Randall, "Highly robust error correction by convex programming," *IEEE Trans. Inf. Theory*, vol. 54, no. 7, pp. 2829–2840, July 2008.

[39] E. Candes and M. Wakin, "An introduction to compressive sampling," *IEEE Signal Process. Mag.*, vol. 25, no. 2, pp. 21–30, 2008.

[40] M. Chitre, S. Ong, and J. Potter, "Performance of coded ofdm in very shallow water channels and snapping shrimp noise," in *OCEANS, 2005. Proc. of MTS/IEEE*, 2005, pp. 996–1001 Vol. 2.

[41] M. Chitre, S. Kuselan, and V. Pallayil, "Ambient noise imaging in warm shallow waters; robust statistical algorithms and range estimation," *The J. of the Acoustical Soc. of Amer.*, vol. 132, no. 2, 2012.

[42] D. Ojeda, "Comparative study of stable parameter estimators and regression with stably distributed errors," Ph.D. dissertation, American Univ., 2001.

**Ahmed Mahmood** (GM'12) received his B.Eng and M.Eng degrees in electrical engineering from the National University of Sciences and Technology (NUST), Pakistan, and a Ph.D. degree from the Department of Electrical & Computer engineering, National University of Singapore (NUS), Singapore. In 2014, Dr. Mahmood joined the Acoustic Research Laboratory (ARL) at NUS, where he is now a Research Fellow. He has served as a reviewer for the IEEE Transactions on Communications and IET Communications. His current research interests involve underwater acoustic communications, robust signal processing, channel modelling, estimation & detection theory and error correction coding for impulsive noise.

**Mandar Chitre** (M'03–SM'12) received B.Eng. and M.Eng. degrees in electrical engineering from the National University of Singapore (NUS), Singapore, a M.Sc. degree in bioinformatics from the Nanyang Technological University (NTU), Singapore, and a Ph.D. degree from NUS. From 1997 to 1998, he worked with the ARL, NUS in Singapore. From 1998 to 2002, he headed the technology division of a regional telecommunications solutions company. In 2003, he rejoined ARL, initially as the Deputy Head (Research) and is now the Head of the laboratory. Dr. Chitre also holds a joint appointment with the Department of Electrical & Computer Engineering at NUS as an Assistant Professor. His current research interests are underwater communications, autonomous underwater vehicles and acoustic signal processing.

Dr. Chitre has served on the technical program committees of the IEEE OCEANS, WUWNet, DTA and OTC conferences and has served as reviewer for numerous international journals. He was the chairman of the student poster committee for IEEE OCEANS06 in Singapore, and the chairman for the IEEE Singapore AUV Challenge 2013. He is currently the IEEE Ocean Engineering Society technology committee co-chair of underwater communication, navigation & positioning.

**Marc A. Armand** (M'00-SM'07) received his B.Eng and Ph.D. degree in electrical engineering from the University of Bristol, U.K., in 1995 and 1999, respectively. He is currently an Associate Professor at the Department of Electrical and Computer Engineering, National University of Singapore, which he joined in Dec 2000 as an Assistant Professor. He is a Senior Member of the IEEE and has published over 50 journal and conference papers in the area of coding theory and techniques, as well as detection, coding and channel modelling for magnetic recording and underwater communications.